Mon. Not. R. Astron. Soc. **330,** 855–875 (2002)

Photometric modelling of slowly pulsating B stars

R. H. D. Townsend★

Department of Physics & Astronomy, University College London, Gower Street, London WC1E 6BT

Accepted 2001 November 3. Received 2001 October 30; in original form 2001 June 30

ABSTRACT

The photometric characteristics of slowly pulsating B stars are investigated using a numerical approach. Stability calculations are performed for a set of stellar models representative of the mid-B type, using a non-radial non-adiabatic pulsation code. The results from these calculations are used to synthesize photometry, in several common systems, for unstable modes of harmonic degrees $\ell = 1...4$. Focusing on the Geneva system for illustrative purposes, a variety of techniques are employed to analyse and visualize the synthetic data, including the use of multicolour-amplitudes and amplitude–phase diagnostic diagrams. One outstanding aspect of the analysis is the discovery, for the $\ell = 2...4$ modes, of 'inter-term cancellation' (ITC) – the process of destructive interference between the flux variations originating from surface temperature perturbations and those arising from radius perturbations.

The ITC can be severe enough that a mode may be excited to a significant amplitude, and yet exhibit levels of photometric variability that fall below typical observational detection thresholds. Furthermore, it can affect not only the light variations in a given photometric passband, but also the variations of the bolometric flux. However, the cancellation is dependent on wavelength, and will not occur to the same degree in more than one passband. Therefore, simultaneous observation in a multitude of passbands represents the best approach to ensuring that no modes are overlooked during searches for variability in B-type stars.

A consequence of ITC is that ratios between the variability amplitude, in differing passbands, become very sensitive towards mode-to-mode changes in the pulsation. This increased sensitivity will tend to complicate any attempts at identifying the harmonic degrees of the modes responsible for observed variability. However, the cancellation also introduces significant phase differences between the light variations in each passband, especially for the $\ell = 3$ and $\ell = 4$ modes. On the grounds that correspondingly large phase differences are not seen in observational data, it is argued that the variability seen in slowly pulsating B stars can tentatively be attributed to $\ell = 1$ and $\ell = 2$ modes.

Key words: methods: observational – techniques: photometric – stars: early-type – stars: oscillations – stars: variables: other.

1 INTRODUCTION

Much of the recent interest in early-type stellar variability has been directed toward the slowly pulsating B-type (SPB) stars. First introduced as a distinct class by Waelkens (1991), these systems exhibit multiperiodic, long-time-scale (∼1–5 d) light and colour fluctuations, and have been identified as the photometric counterparts to the 53 Per spectroscopically variable pulsators discovered by Smith (1977). Theoretical studies (see e.g. Pamyatnykh 1999, and references therein) indicate that the κ-mechanism excitation of multiple non-radial g modes, arising from a metal-line opacity bump at a temperature $T \sim 2 \times 10^5$ K, can explain the SPB phenomenon. Although there remains some uncertainty regarding the physical nature of mode selection (Dziembowski, Moskalik & Pamyatnykh 1993), the close agreement between the observed and predicted instability domains in the Hertzprung–Russell diagram (Pamyatnykh 1999, his figs 3 and 4) indicates that the SPB class is well understood.

With the unanticipated discovery by the *Hipparcos* satellite of a large number (∼100) of new candidate SPB stars (Waelkens et al. 1998), and looking forward to upcoming space-based missions (Eyer 2000), which may reveal even more members of the class, these systems will soon be within the reach of statistical analysis techniques (Gautschy 2000). First, however, it will be necessary to

★E-mail: rhdt@star.ucl.ac.uk

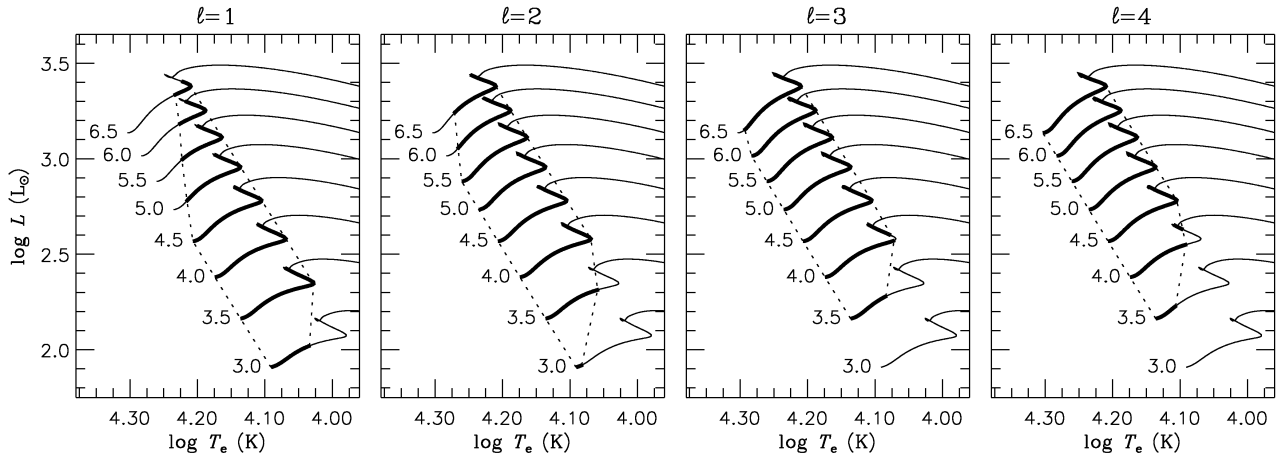

Figure 1. Tracks in the theoretical Hertzprung–Russell diagram for the eight evolutionary sequences of mid-B type stellar models considered throughout. Each track is labelled with the initial stellar mass, in solar units; thick (thin) lines are used to indicate which stages are overstable (stable) against one or more non-radial pulsation modes of the indicated harmonic degree ℓ. The dotted lines indicate the implied boundaries of the SPB instability strip.

secure reliable identification of the g modes responsible for the observed variability. How may these identifications be made? One approach is the modified Baade–Wesselink technique devised by Dziembowski (1977), which permits the inference of the harmonic degree ℓ of a mode from light and radial velocity observations. The technique has been improved by a number of authors (e.g. Buta & Smith 1979; Balona & Stobie 1979), and Stamford & Watson (1981) have adapted it for use with multicolour photometric measurements alone. It has been deployed successfully by both Heynderickx, Waelkens & Smeyers (1994) and Cugier, Dziembowski & Pamyatnykh (1994) in the analysis of β Cepheid stars, the higher luminosity cousins to the SPBs.

The outstanding aspect of the last authors' treatment was the incorporation of quantitative theoretical data, derived from stability calculations, which describe the non-adiabatic character of pulsation at the stellar surface. In the case of early-type stars, reliable values for these data have become available only since the discovery of the metal-line κ-mechanism instability (Cox et al. 1992; Dziembowski & Pamyatnykh 1993; Dziembowski et al. 1993). Therefore, it is no mystery why prior photometric studies of both β Cepheid and SPB variability were restricted to ad hoc or empirical estimates of non-adiabacity (e.g. Watson 1988; Heynderickx et al. 1994), or to the assumption of completely adiabatic pulsation (e.g. Buta & Smith 1979). Nevertheless, despite of the fact that the non-adiabatic characteristics of SPB pulsators are now well-understood, photometric modelling of these systems, with the quantitative treatment of non-adiabacity, has yet to be undertaken.

This last point is addressed by the present paper, which investigates the theoretically predicted light and colour variations of SPB stars, using an approach similar to that of Cugier et al. (1994). Linear stability calculations are undertaken for a large number of mid-B type stellar models, producing parameters which characterize the photospheric perturbations resulting from each overstable non-radial mode. These parameters are combined with line-blanketed model atmospheres to obtain light curves in a number of passbands for the overstable modes. Details of the method are presented in the following section, while Section 3 is devoted to analysis of the resulting synthetic data. In Section 4, these data are compared with recent observations of SPB variability; conclusions for the entire paper are then drawn in Section 5.

2 METHOD

2.1 Stellar models

The Warsaw–New Jersey evolutionary code[1] was used to calculate eight tracks of mid-B type stellar models, uniformly sampling the initial mass range $M = 3.0\,\mathrm{M}_\odot$–$6.5\,\mathrm{M}_\odot$, and extending from zero-age main sequence to somewhat beyond the cessation of core hydrogen burning. Details of this code have already been given by Dziembowski & Pamyatnykh (1993) and Dziembowski et al. (1993); the only significant difference in the present work was the adoption of more-recent OPAL tabulations for opacity (Iglesias & Rogers 1996) and equation of state (Rogers, Swenson & Iglesias 1996). In all cases, the initial hydrogen and metal mass fractions were set at $X = 0.7$ and $Z = 0.02$, respectively, with a heavy-element mixture taken from Grevesse & Noels (1993).

Fig. 1 shows the evolutionary tracks, for each initial mass, in the theoretical Hertzprung–Russell diagram. The thickness of the track lines has been used to indicate the vibrational stability of the models against the excitation of non-radial modes with harmonic degrees $\ell = 1\ldots4$. Details of the stability calculations are discussed in the following section.

2.2 Stability calculations

Stability calculations for all stellar models were undertaken using NARK, a new finite-difference relaxation code for solution of the full system of linear, non-radial, non-adiabatic pulsation equations. The implementation of NARK is based largely on the detailed descriptions given by Unno et al. (1989), with an outer mechanical boundary condition taken from Dziembowski (1971). Perturbations to the convective flux are neglected throughout (the so-called 'frozen convection' approximation), and radiative heat transfer is treated within the Eddington approximation (see Ando & Osaki 1975). As discussed by Unno & Spiegel (1966), the latter is exact in both the optically thick and optically thin limits, and reasonably accurate across intermediate regions. Mesh points are inserted automatically, to ensure adequate resolution of the spatial oscillation of eigenfunctions, and the accuracy of solutions is checked using the work-integral technique of Ando & Osaki (1975).

[1] Kindly provided by R. Sienkiewicz.

The overall normalization of eigenfunctions, regarding which the linear formalism can say nothing, has a direct bearing on predicted variability amplitudes, and must be selected with some care. Although a full non-linear theory for modal limiting amplitudes has yet to be developed, Dziembowski et al. (1993) have suggested a simple yet physically reasonable approach to the problem, based around the assumption that amplitude limitation arises from non-linear saturation of the κ-mechanism driving. This approach, adopted within NARK, may be expressed by the requirement that the relative Lagrangian perturbation δT to the temperature T satisfies

$$\left\langle \left| \frac{\delta T}{T} \right|^2 \right\rangle = 0.1 \tag{1}$$

in the driving zone, where $\langle \ldots \rangle$ denotes the average over all solid angles. Dziembowski et al. (1993) chose to apply this condition at a constant fraction (96 per cent) of the stellar radius; however, NARK implements a more flexible approach, invoking the requirement (1) at the peak of the metal-line opacity bump.

Results from the stability calculations, for harmonic degrees $\ell = 1 \ldots 4$, are summarized in Fig. 1. Exploratory calculations indicated that higher degree ($\ell \geqslant 5$) modes generate light variations at very low levels ($\lesssim$2.5 mmag), and cannot therefore be considered a significant source of SPB photometric variability. The implied boundaries of the SPB instability strip shown in the figure, located at zero- and terminal-age main sequence, exhibit good agreement with those presented by Pamyatnykh (1999).

The principal goal of the stability calculations was to obtain parameters describing the perturbative influence of each overstable mode upon the stellar photosphere. Let the time-dependent relative Lagrangian perturbation δy to a given variable y, at the stellar surface, be expressed in the canonical form

$$\frac{\delta y}{y} = \mathrm{Re}[Y_\ell^m(\theta, \phi)\, \mathrm{e}^{\mathrm{i}\sigma t} \Delta_y], \tag{2}$$

where Y_ℓ^m is the spherical harmonic of the appropriate harmonic degree ℓ and azimuthal order m, and Re[...] denotes the real part. The complex coefficient Δ_y, which completely characterizes the perturbation, is found from the stability calculations as the surface value of the corresponding radius-dependent eigenfunction $(\delta y/y)(r)$. In the present case, the coefficients obtained for every overstable mode were Δ_p, Δ_T and Δ_R, describing respectively the perturbations to the photospheric pressure p, effective temperature T_e and stellar radius R. Together with the eigenfrequency σ, they represent the data required for photometric modelling of any given mode.

Before discussing the method adopted for this modelling, it is instructive to compare the results of the non-adiabatic calculations with the predictions of adiabatic pulsation theory. Fig. 2 shows the complex modulus and argument of Δ_T – the effective temperature coefficient – as a function of pulsation period $\Pi \equiv 2\pi/\sigma$, for the unstable $\ell = 2$ modes of an $M = 4.0$-$\mathrm{M}_\odot$ stellar model, the parameters of which are specified in Table 1. This model was chosen to coincide loosely with the one examined in detail by Dziembowski et al. (1993), and will be used for illustrative purposes throughout the present investigation. Also shown in the figure are the corresponding data predicated by the adiabatic approximation,

$$\Delta_T = \nabla_\mathrm{ad} \Delta_p \tag{3}$$

(Buta & Smith 1979), and those for the radius perturbation coefficient Δ_R; here, ∇_ad is the adiabatic temperature gradient within the photosphere.

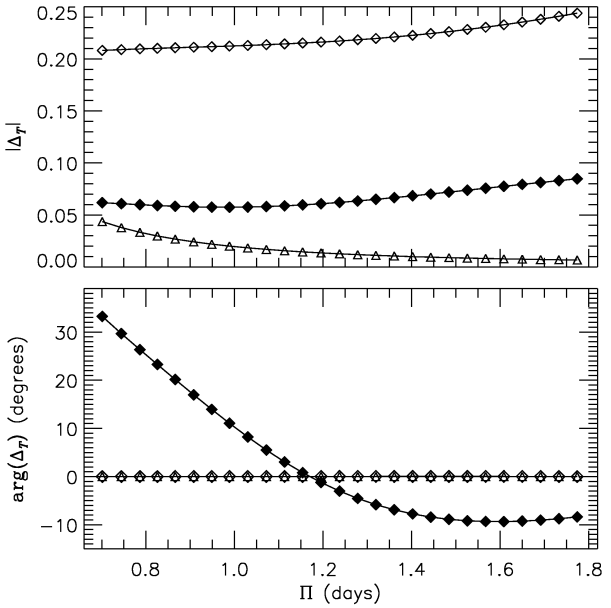

Figure 2. The modulus and phase of Δ_T, the effective temperature perturbation coefficient, as a function of pulsation period Π for the unstable $(g_{16} \ldots g_{42})$ $\ell = 2$ modes of the 4-$\mathrm{M}_\odot$ stellar model specified in Table 1. Filled (open) diamonds show the results obtained with non-adiabatic (adiabatic) theory, while open triangles indicate the corresponding values for Δ_R, the surface radius perturbation coefficient.

Table 1. The mass M, radius R, luminosity L, effective temperature $\mathrm{T_e}$ and central hydrogen mass fraction $\mathrm{X_c}$ of the stellar model considered within the text and subsequent figures.

M ($\mathrm{M}_\odot$)	R ($\mathrm{R}_\odot$)	$\log L$ ($\mathrm{L}_\odot$)	$\log T_\mathrm{e}$ (K)	X_c
4.00	3.40	2.50	4.12	0.37

The figure demonstrates that – as found by Cugier et al. (1994) for the β Cephei pulsators (and see also Dupret 2001) – the adiabatic approximation is decidedly inadequate in the context of SPB stars: the amplitude of temperature perturbations is consistently overestimated by a factor $\sim$3, and the phase lags between Δ_T and Δ_R are not reproduced correctly. This result is hardly surprising, because the thermal time-scale in the photospheres of the latter systems ($\sim$12.4 min in this particular case) is very much shorter than typical pulsation periods, and significant heat exchange between neighbouring fluid parcels is to be expected. With this fact in mind, the continued use of the adiabatic approximation for SPB modelling should certainly be discouraged.

2.3 Photometric modelling

Expanding on previous work by Dziembowski (1977) and others, Watson (1987) introduced a useful semi-analytical model for the flux variations resulting from a non-radial mode, which includes the first-order contributions from temperature, pressure and radius perturbations. Adopting this model, suitably modified for the present parametrization scheme, the time-dependent perturbation $\delta \mathcal{F}_x$ to the observed flux $\mathcal{F}_x$ in some photometric passband

(denoted by the subscript x) is expressed as

$$\frac{\delta\mathcal{F}_x}{\mathcal{F}_x} = \mathrm{Re}\left\{ Y_\ell^m(\Theta,\Phi)\,\mathrm{e}^{\mathrm{i}\sigma t} \times\left[\frac{\Delta_p}{\mathcal{I}_{0x}}\frac{\partial}{\partial\ln g}+\frac{\Delta_T}{\mathcal{I}_{0x}}\frac{\partial}{\partial\ln T_\mathrm{e}}+\frac{\Delta_R}{\mathcal{I}_{0x}}(2+\ell)(1-\ell)\right]\mathcal{I}_{\ell x}\right\}, \quad (4)$$

where $\{\Delta_p,\ \Delta_T,\ \Delta_R\}$ are the complex amplitude coefficients introduced in the preceding section, (Θ,Φ) are the spherical-polar coordinates of the sub-observer point, and $g \equiv GM/R^2$ is the surface gravity of the star. The term $\mathcal{I}_{\ell x}$ depends on the radiation field of the equilibrium photosphere, and is defined, for a given ℓ and x, by

$$\mathcal{I}_{\ell x} = \int_0^\infty \left[\int_0^1 \mathcal{I}(\lambda,\mu)P_\ell(\mu)\mu\,\mathrm{d}\mu\right]\mathcal{S}_x(\lambda)\,\mathrm{d}\lambda; \quad (5)$$

here, $\mathcal{I}(\lambda,\mu)$ is the specific intensity at wavelength λ and cosinus μ to the local surface normal, which is obtained from static model atmospheres. Furthermore, $P_\ell(\mu)$ is the Legendre polynomial of degree ℓ, and $\mathcal{S}_x(\lambda)$ is the overall response function of photometric band x, combining the individual contributions from atmosphere, telescope, filter and detector. With these definitions, $\mathcal{I}_{\ell x}$ is related to Watson's (1988) weighted limb-darkening integral $b_{\ell\lambda}$ through

$$\mathcal{I}_{\ell x} = \mathcal{I}_{0x}\int_0^\infty b_{\ell\lambda}\mathcal{S}_x(\lambda)\,\mathrm{d}\lambda, \quad (6)$$

where $\mathcal{I}_{0x}$, being the value of $\mathcal{I}_{\ell x}$ for $\ell = 0$, is proportional to the total flux $\mathcal{F}_x$ in band x.

In the derivation of equation (4), the approximation

$$\frac{\partial\mathcal{I}_{\ell x}}{\partial\ln p} = \frac{\partial\mathcal{I}_{\ell x}}{\partial\ln g} \quad (7)$$

was adopted when considering the light variations engendered by pressure perturbations. This approximation is useful because the radiation field is more naturally parametrized by surface gravity than by photospheric pressure. It is reasonably accurate for hot stars (Watson 1988, and references therein), and becomes exact when the radial gradient of $\delta p/p$ is negligible within the photosphere (Cugier et al. 1994; Balona & Evers 1999). In the present work, the latter condition is implicitly enforced, for all modes, by the adoption (Section 2.2) of Dziembowski's (1971) outer mechanical boundary condition (see e.g. Townsend 1997 for proof). Therefore, the incorporation of the approximation (7) does not degrade the physical realism of the modelling any further. In any case, pressure perturbations typically contribute little towards the light variations of SPB stars (see Section 3.1), and the accuracy of the approximation will be of secondary importance in the majority of cases.

To widen the generality of results, it is useful to remove from equation (4) the dependence of $\delta\mathcal{F}_x$ on the arbitrary sub-observer coordinates (Θ,Φ) and azimuthal order m. This is readily achieved by replacing the $Y_\ell^m(\Theta,\Phi)$ term in the equation with an appropriate average

$$\bar{Y}_\ell = \frac{1}{2\ell+1}\sum_{m=-\ell}^{\ell}\frac{1}{4\pi}\int_0^{2\pi}\int_0^{\pi}|Y_\ell^m(\Theta,\Phi)|\sin\Theta\,\mathrm{d}\Theta\,\mathrm{d}\Phi \quad (8)$$

over all aspect angles and permissible azimuthal orders. The flux variations are then expressed as

$$\frac{\overline{\delta\mathcal{F}_x}}{\mathcal{F}_x} = \bar{Y}_\ell\,\mathrm{Re}\left\{\mathrm{e}^{\mathrm{i}\sigma t}\left[\frac{\Delta_p}{\mathcal{I}_{0x}}\frac{\partial}{\partial\ln g}+\frac{\Delta_T}{\mathcal{I}_{0x}}\frac{\partial}{\partial\ln T_\mathrm{e}} +\frac{\Delta_R}{\mathcal{I}_{0x}}(2+\ell)(1-\ell)\right]\mathcal{I}_{\ell x}\right\}, \quad (9)$$

which is independent of both m and (Θ,Φ). In those situations where a star has a particularly favourable orientation (i.e. when $|Y_\ell^m(\Theta,\Phi)|$ is maximal), the latter expression can significantly underestimate the flux variations; Table 2 details the worst-case scenarios for all $\ell \leqslant 4$ non-radial modes. Nevertheless, when modelling a large ensemble of stars, with randomized orientation and azimuthal degree, equation (9) should lead to statistically valid results. A similar averaging technique was adopted by Balona & Dziembowski (1999) for the purpose of establishing upper limits on the photometric amplitude of δ Scuti stars.

Table 2. The factors, for each appropriate value of ℓ and $|m|$, by which photometric modelling using averaged spherical harmonics $\bar{Y}_\ell$ (equation 8) will, ceteris paribus, underestimate the flux variations from a star aligned in the most favourable orientation.

		$\lvert m\rvert$				
		0	1	2	3	4
ℓ	1	1.86	1.32			
	2	2.48	1.52	1.52		
	3	2.99	1.78	1.57	1.70	
	4	3.43	2.03	1.74	1.65	1.80

For the unstable modes found by NARK, equation (9) was used to synthesize photometry in the Johnson–Cousins, Strömgren, Geneva and *Hipparcos* photometric systems. Response functions $\mathcal{S}_x(\lambda)$ for the passbands of these systems were obtained from Bessell (1990), Matsushima (1969), Rufener & Nicolet (1988) and Perryman (1997), respectively; where necessary, data for atmospheric extinction and the reflectivity of aluminium were taken from the tabulations by Allen (1976). Specific intensity data $\mathcal{I}(\lambda,\mu)$, and their appropriate partial derivatives, were linearly interpolated in an ATLAS9 grid of local thermodynamic equilibrium (LTE) line-blanketed synthetic spectra (Kurucz 1993), at solar abundance and 2 km s^{-1} microturbulent velocity.

Each resulting periodic light curve was characterized by its cosinusoidal semi-amplitude $\mathcal{A}_x$ and phase φ_x relative to the nominal $t = 0$ epoch of equation (9). As almost all observations of SPB stars have been undertaken in the Geneva photometric system (e.g. Waelkens & Rufener 1985; Waelkens 1991; North & Paltani 1994; Waelkens et al. 1998; De Cat & Aerts, in preparation) the focus of subsequent sections is placed almost wholly on the presentation and analysis of the data in the Geneva $UB_1BB_2V_1VG$ passbands. However, the amplitude and phase data of *all* photometric systems considered have been made available for download from the World Wide Web, at http://www.star.ucl.ac.uk/~rhdt/download/

3 RESULTS

3.1 Light variations in the *V* band

Fig. 3 shows the Geneva V-band light amplitude $\mathcal{A}_V$ as a function of mode period Π and central hydrogen mass fraction X_c, for each

harmonic degree and evolutionary sequence considered. Although the mode spectrum at a given X_c is discrete, linear interpolation has been used to represent $\mathcal{A}_V$ as a continuous function of Π. Across those regions of the $\Pi - X_c$ plane where the stellar configuration is stable against pulsation, $\mathcal{A}_V$ has been set identically to zero.

The synthetic data plotted in the figure can be regarded as theoretical upper limits for the *V*-band light variations across the SPB instability strip; however, the approximations and assumptions adopted during the modelling should be borne in mind when applying such an interpretation. As discussed in the preceding section, the use of angle-averaged spherical harmonics $\overline{Y}_\ell$ when calculating $\overline{\delta\mathcal{F}_x}$ (equation 9) is appropriate only when considering the mean properties of an ensemble of pulsating stars. Moreover, it has been assumed that amplitude limitation occurs through saturation of the opacity-mechanism driving. Even if this assumption is correct, the normalization condition (1) is valid only for monomodal pulsation; the simultaneous excitation of two or more modes will lead to a corresponding reduction in the variability generated by each one (see Dziembowski et al. 1993).

The most prominent feature of Fig. 3, for all stellar models, is the rapid decline of the flux variations with increasing harmonic degree: at $\ell = 1$, the maximal averaged light amplitude is $\mathcal{A}_V \approx 49$ mmag, but for $\ell = 2, 3, 4$ it falls to $\mathcal{A}_V \approx 23, 5, 10$ mmag, respectively. This behaviour, endemic to non-radial pulsation, arises from partial cancellation between regions of the stellar disc oscillating in antiphase with one another. Towards larger values of ℓ, the disc is subdivided into an ever-increasing number of these regions, and the cancellation becomes correspondingly more complete. Disc-averaging cancellation was first considered by Dziembowski (1977), who demonstrated that the weighted limb-darkening coefficient $b_{\ell\lambda}$ is asymptotically proportional to $\ell^{-2.5}(\ell^{-3.5})$ for modes of even (odd) harmonic degree. The same dependence is exhibited by the radiation-field term $\mathcal{I}_{\ell x}$ in equation (9), owing to the inter-relationship (6) between $b_{\ell\lambda}$ and $\mathcal{I}_{\ell x}$; accordingly, even with the growth of other ℓ-dependent terms in the former equation, the flux variations will decline along each sequence of even- or odd-ℓ modes, the decline being most rapid in the latter. Judging from the figure – which, it should be recalled, provides upper limits on the anticipated light amplitude of SPB stars – it would appear that $\ell = 3$ or $\ell = 4$ modes will be hard pushed to generate variability at amplitudes approaching those observed in SPB stars.

The other aspect of Fig. 3 warranting attention is the appearance, most obvious in the intermediate-mass $\ell = 2$ panels, of pronounced 'valleys' in the light-amplitude data. These valleys – minima of $\mathcal{A}_V$ with respect to Π – are a consequence of what shall be termed *inter-term cancellation* (ITC). In contrast to the disc-averaging cancellation of the foregoing discussion, ITC is the process of destructive interference between contributions towards the light variations arising from each type of photospheric perturbation. Two separate factors conspire to produce ITC in SPB stars. First, temperature and radius perturbations in these systems vary approximately in phase, as can be appreciated from the Δ_T and Δ_R data plotted in Fig. 2. This is a general characteristic of g-mode pulsation, for which the regions of maximum compression – and hence, maximum heating – tend to occur where the stellar surface is displaced outwards. Because the $(2 + \ell)(1 - \ell)$ term in equation (9) is negative when $\ell \geqslant 2$, the flux changes from temperature and radius perturbations are then in approximate antiphase, opening up the possibility of destructive interference between the two.

Secondly, temperature perturbations in SPB stars result primarily from horizontal compression of the photospheric gas. The relative strength of the compression grows with increasing pulsation period; therefore, while the light variations of shorter period modes are primarily generated by radius perturbations, those of the longer period modes arise from the increasingly dominant temperature perturbations. At some intermediate period, the two perturbations will make approximately equal contributions towards the variability; as these contributions are in antiphase, a minimum in the light amplitude will result.

To illustrate the foregoing discussion, Fig. 4 plots the *V*-band light amplitude $\mathcal{A}_V$ and phase φ_V as a function of period, for $\ell = 2$ modes of the 4.0-$M_\odot$ model introduced in Table 1. Also shown in the figure are the individual contributions towards the variability from the pressure, temperature and radius perturbations; these contributions may be identified with the terms in equation (9) proportional to Δ_p, Δ_T and Δ_R, respectively. Evidently, although the radius contribution is strongest at the short-period limit, that of the temperature perturbations becomes more and more significant as the period is increased. Approaching $\Pi \sim 1$ d, the two are approximately equal in magnitude; however, their phases differ by nearly 180°, and they thus combine in opposition to produce a distinct minimum in the total light amplitude $\mathcal{A}_V$. Observe that the pressure contribution, accounting for only a tiny fraction of the variability, plays little part in the process; this latter result holds for the vast majority of modes studied, but – as will be discussed subsequently – there exist a few situations where the pressure contribution can play a significant role.

If the radius and temperature contributions were in precise antiphase, the light variations would vanish completely at the period where their magnitudes are equal. In physically realistic situations, however, total cancellation rarely occurs: non-adiabatic processes at the stellar surface introduce a small phase lag between Δ_T and Δ_p (see Fig. 2), which means that the phase difference between the two corresponding contributions deviates somewhat from 180°. The size of this deviation plays a role in determining the minimum value of $\mathcal{A}_V$ attained, and – to a much lesser part – the period at which the minimum will occur.

Returning to Fig. 3, minima in the $\ell = 2$ amplitude data resulting from ITC are evident in the intermediate and higher mass ($M = 4.0 - 6.5\,M_\odot$) evolutionary sequences. Along each sequence, the increasing stellar luminosity promotes ever-larger departures from adiabacity within the photospheres of the models (see Unno et al. 1989, section 22.1), which tend to dilute the temperature perturbations. As a consequence, the period of the $\mathcal{A}_V$ minimum lengthens as the models evolve from zero- to terminal-age main sequence. A similar lengthening is also seen in the short- and long-period boundaries of the κ-mechanism instability, owing to the growth in the dynamical time-scale of the models. Taken together, these two effects mean that the positioning of the $\mathcal{A}_V$ minima, relative to the boundaries of the instability, remains largely unaffected by evolutionary processes.

For the unstable $\ell = 3$ and $\ell = 4$ modes shown in Fig. 3, ITC also occurs, but tends to be most pronounced very close to the long-period boundaries of the instability. Therefore, rather than appearing as a distinct minimum in the light amplitude, as for the $\ell = 2$ modes, cancellation in the higher order modes manifests itself as a decline in the light amplitude with increasing pulsation period. This decline is so rapid that the *V*-band light amplitude of the unstable, longest-period $\ell = 3$ ($\ell = 4$) modes did not exceed 1.32 mmag (1.60 mmag) in any of the stellar models considered – values which are well below the typical detection thresholds of current ground-based observing facilities.

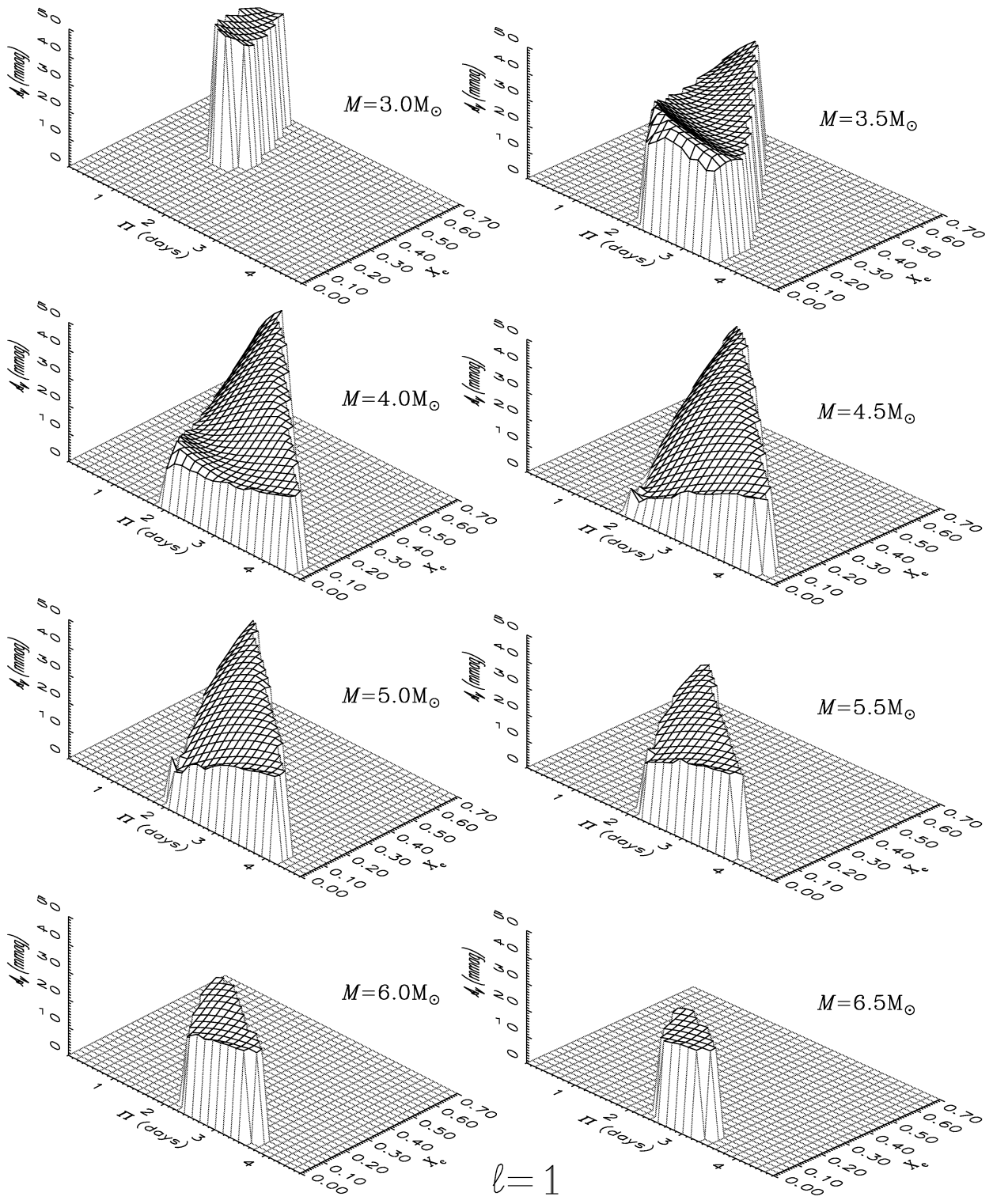

Figure 3. The cosinusoidal semi-amplitude $\mathcal{A}_V$ (in mmag) of light variations in the Geneva *V*-band, as a function of pulsation period Π and central hydrogen abundance X_c, for the unstable $\ell = 1, 2, 3$ and 4 modes, of the eight evolutionary sequences considered throughout. Note the different vertical scaling for each ℓ.

Unlike the situations outlined above, cancellation between the temperature and radius contributions never arises for $\ell = 1$ modes. This is because the $(2+\ell)(1-\ell)$ term in equation (9) is identically zero, and the radius contribution vanishes. However, in the rare cases where the temperature perturbations are very small, the normally unimportant photospheric pressure perturbations can become a significant contributor towards the light variations. Under these circumstances, ITC can arise between the temperature

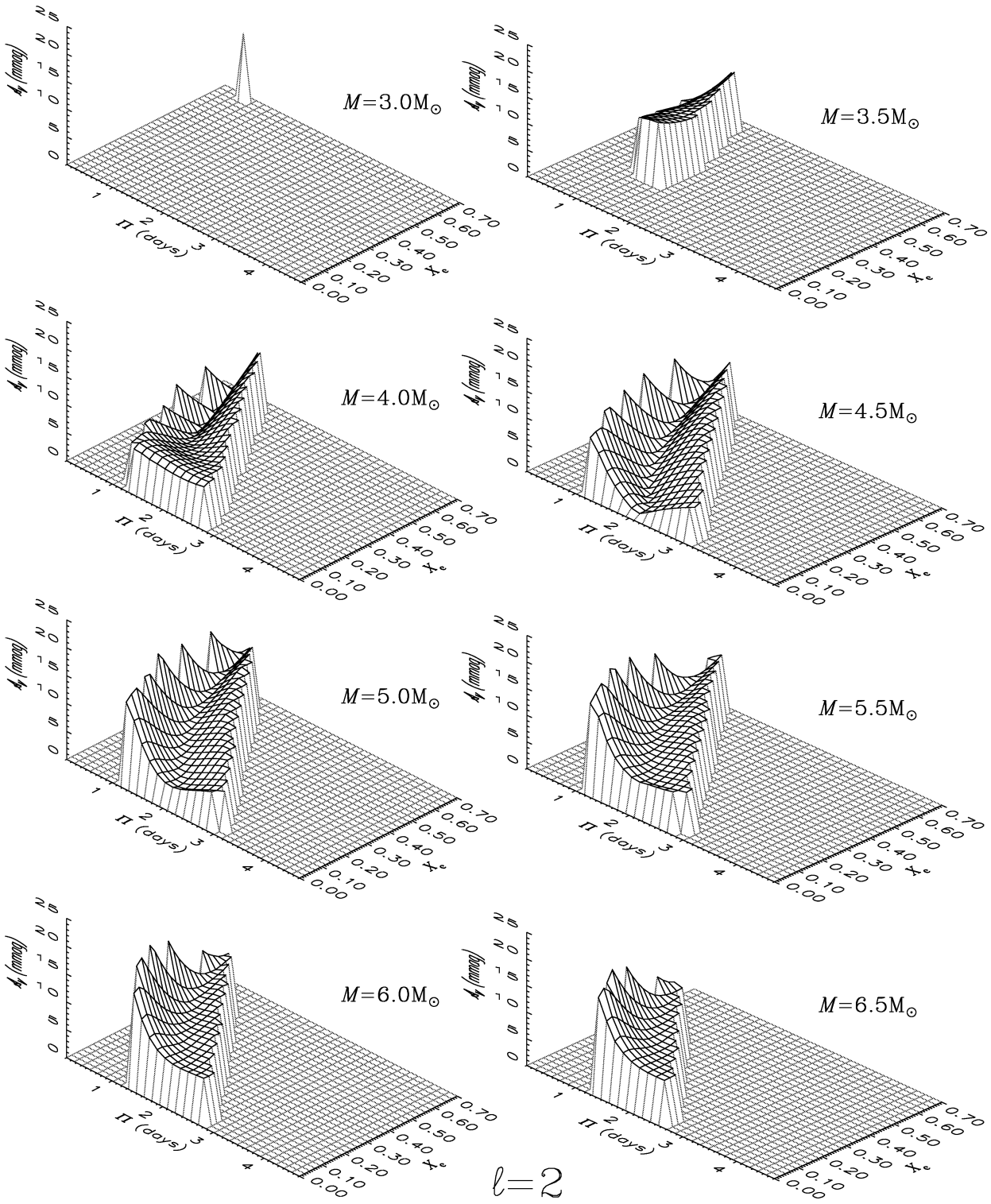

Figure 3 – *continued*

and pressure contributions; such scenarios will be encountered in subsequent sections.

On a historical note, it should be mentioned that ITC was first considered – albeit not under the present name – by Watson (1987), who correctly surmised that g-mode radius and temperature perturbations might contribute oppositely to the light variations of mid-B type stars, and that these respective contributions could interfere destructively. The strength of the present analysis lies in the fact that it does not rely – as Watson (1987) had to – on estimates of the temperature perturbations in the presence of non-adiabatic processes. Inaccuracies in these estimates can have a profound effect on the predicted nature and

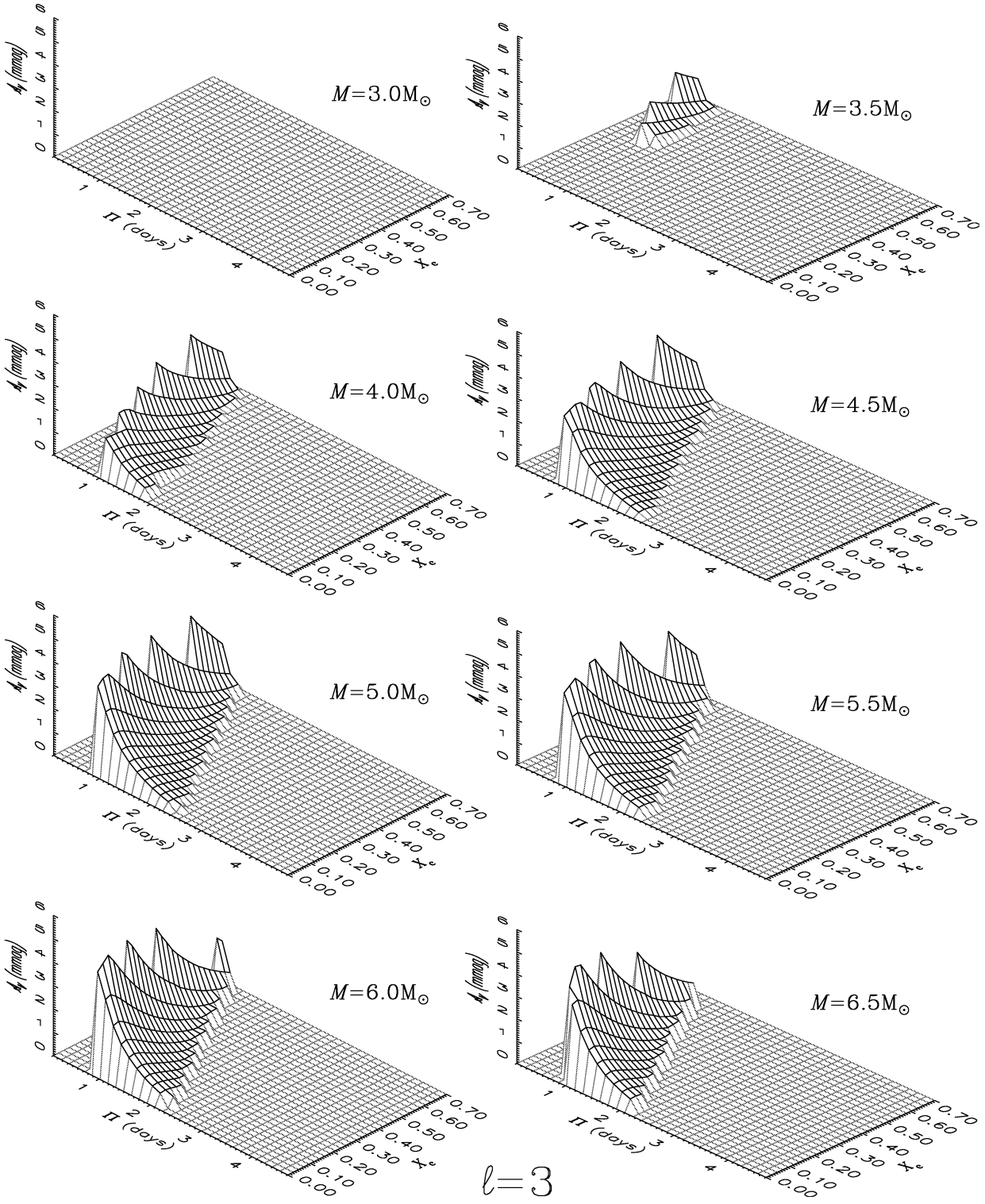

Figure 3 – *continued*

incidence of ITC, and lead to misleading results even at a qualitative level.

3.2 Light variations in other bands

Based on previous observational studies, North & Paltani (1994) suggested that SPB variability may be characterized by an inverse dependence between light amplitude and wavelength, and the absence of any significant phase lags between the variations in differing photometric bands. To examine whether this characterization applies to the synthetic data, the discussion is now expanded to consider the variability across the Geneva-system

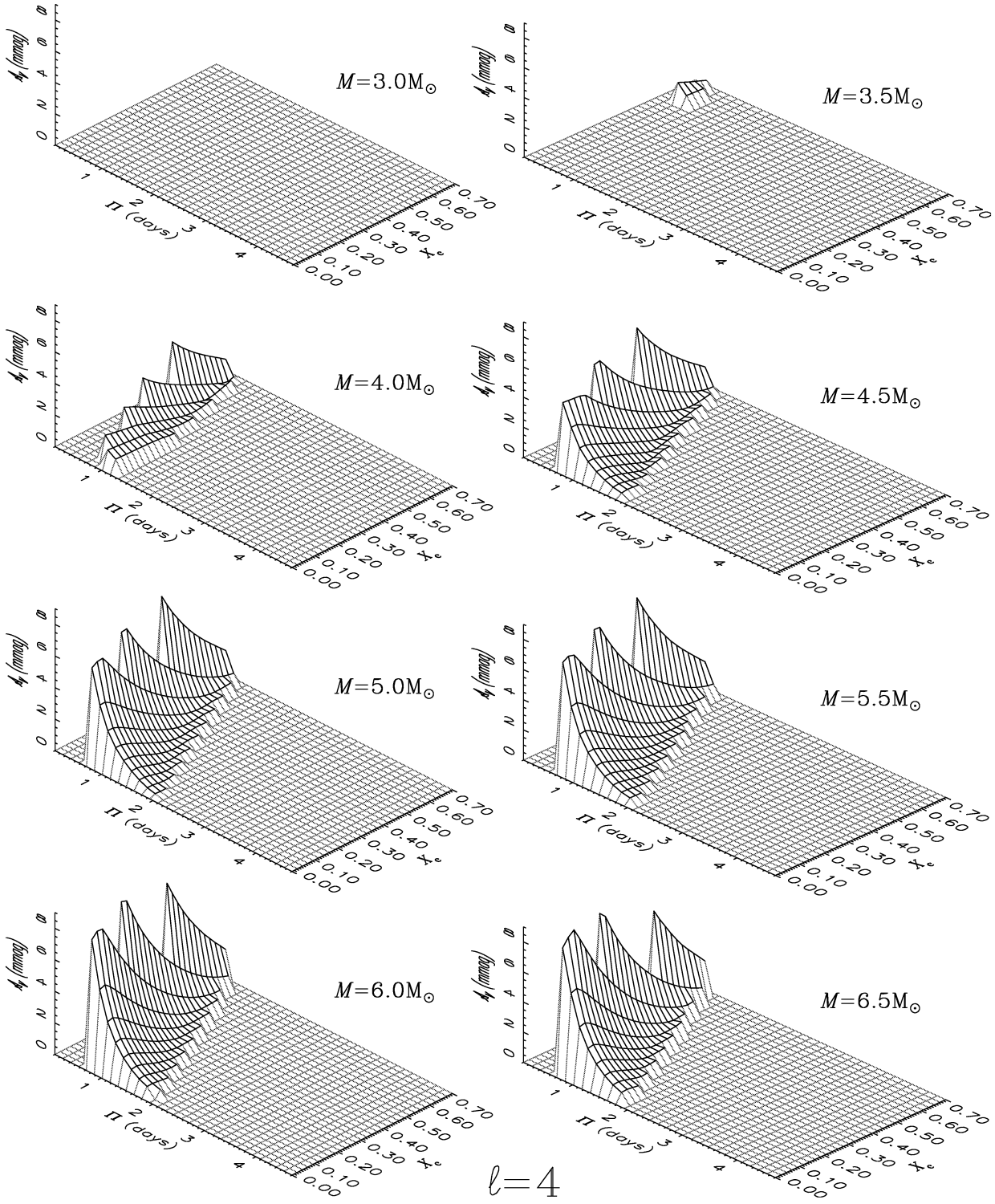

Figure 3 – *continued*

passbands. The present section focuses on the 4.0-$M_\odot$ model introduced previously, which illustrates well the behaviour of many of the other models; the properties of the complete data set are then examined in the following two sections.

Fig. 5 plots, as a function of period, the light amplitudes $\{\mathcal{A}_U, \mathcal{A}_B, \mathcal{A}_V\}$ in the Geneva $\{U, B, V\}$ broadband filters, for the unstable $\ell = 1\ldots4$ modes of the model. Evidently, the behaviour noted by North & Paltani (1994) is best reproduced by the $\ell = 1$ modes: across the blue-to-red sequence of passbands, the light variations decline in amplitude and yet remain ostensibly in phase. This result can readily be understood by considering a hypothetical star in which temperature perturbations alone contribute towards the variability. Inspection of equation (9) reveals that the phase of the light variations in this system will be completely independent

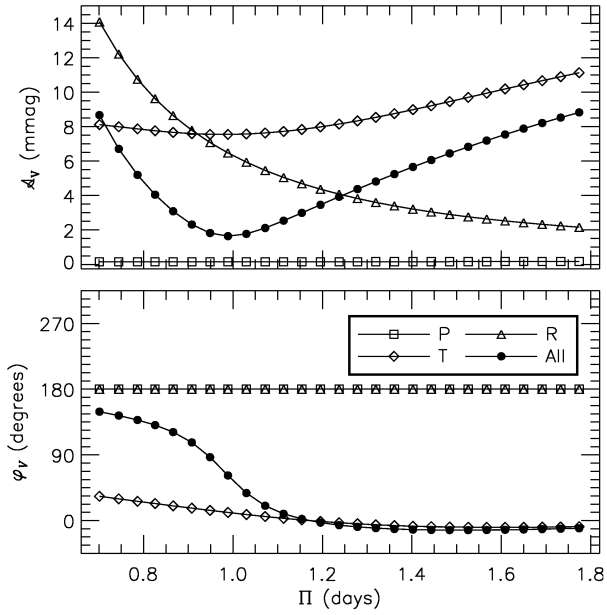

Figure 4. The cosinusoidal semi-amplitude $\mathcal{A}_V$ and phase φ_V (filled circles), as a function of pulsation period Π, of the Geneva *V*-band light variations resulting from unstable $\ell = 2$ modes of the 4-$M_\odot$ stellar model. Individual contributions from perturbations to pressure (squares), temperature (diamonds) and radius (triangles) are also shown.

of the choice of passband, and will simply reflect the underlying phase $\arg(\Delta_T)$ of the temperature perturbations. Likewise, the *relative* amplitude of the variations – between the differing passbands – will depend only on $\mathcal{I}_{0x}$ and the partial temperature derivative of $\mathcal{I}_{\ell x}$. The partial derivative represents the sensitivity of the photospheric flux towards temperature perturbations; in B-type stars, this sensitivity increases rapidly with decreasing wavelength in the visible and near-UV portions of the spectrum. Therefore, the amplitude of the variability exhibited by the star will be relatively smallest in the redmost Geneva *G* passband, and progressively grow in those passbands situated at ever-shorter wavelengths.

For the $\ell = 1$ modes shown in Fig. 5, the absence of a radius contribution (cf. Section 3.1), and the meagre contribution from pressure perturbations, means that the light variations which they exhibit arise almost wholly from temperature perturbations. Therefore, these modes mirror the behaviour of the hypothetical star introduced above: the light variations remain in phase across the three passbands, and the amplitude ratios, $\mathcal{A}_B/\mathcal{A}_U \sim 0.58$ and $\mathcal{A}_V/\mathcal{A}_U \sim 0.54$, change little from mode to mode. These ratios, measuring the relative amplitudes of the variability between the passbands, reflect the differential sensitivity of the photospheric flux against temperature perturbations.

The situation in the $\ell = 2 \ldots 4$ panels of Fig. 5 is significantly complicated by the incidence of ITC, recognizable from the characteristic minima in the amplitude data of the three passbands. For each value ℓ, the minima are located at shorter periods in the *U* band, and longer periods in the *V* band. This is because, towards shorter wavelengths, the increasing temperature contributions allow those modes with correspondingly larger radius contributions to participate in cancellation, and – as explained in the preceding section – such modes are found at shorter pulsation periods.

The differing locations of the $\{\mathcal{A}_U, \mathcal{A}_B, \mathcal{A}_V\}$ minima mean that the relationships between the variability in each passband can change significantly from mode to mode. This can be seen from the $\ell = 4$ panel of Fig. 5: although the amplitude ratios of the longest-period mode, $\mathcal{A}_B/\mathcal{A}_U = 0.44$ and $\mathcal{A}_V/\mathcal{A}_U = 0.34$, follow the same inverse wavelength dependence noted by North & Paltani (1994), the situation is completely reversed in the shortest-period mode, for which $\mathcal{A}_B/\mathcal{A}_U = 1.24$ and $\mathcal{A}_V/\mathcal{A}_U = 1.35$. Another instructive example can be seen in the $\ell = 3$ panel: at short periods, the variations in each band are almost in phase, but, going towards longer periods, those in the *U* band become almost 180° out of phase with those in the *B* and *V* bands. Only for modes distant from the light minima, such as those at the long-period limit of the $\ell = 2$ panel, are the relationships between the variability in each passband approximately constant from mode to mode.

The data presented in Fig. 5 should demonstrate that ITC is not specific to a particular passband. Nor in fact is it specific to the Geneva photometric system: cancellation of a similar nature was also found in the synthetic data of the Johnson–Cousins, Strömgren and *Hipparcos* systems (cf. Section 2.3). Additionally, calculations using a neutral system, where the transmission function $\mathcal{S}_x(\lambda)$ is independent of wavelength, indicated that ITC is to be expected in the *bolometric* flux variations of SPB stars. Accordingly, the possibility is raised that searches for variability, using observations in a single passband, may overlook many variable stars. To address this problem, multicolour observations must always be adopted as the preferred survey approach.

3.3 Multicolour-amplitude diagnostics

In the preceding section, part of the focus was placed on discussion of the amplitude ratios and phase differences between variations in pairs of passbands. As can be appreciated from equations (4) and (9), these quantities are independent of the sub-observer coordinates (Θ, Φ), the azimuthal order *m*, and the overall excitation amplitude of a given mode. This led Heynderickx et al. (1994) to suggest that a graphical comparison of observed and theoretically derived amplitude ratios, plotted as a function of wavelength for a multiplet of passbands, may serve as a discriminant for the harmonic degree ℓ of a mode. Although the technique has primarily been applied to β Cephei stars, it also appears promising for analysis of SPB stars (see e.g. De Cat & Aerts, in preparation).

Accordingly, the present section investigates the typical properties of the Geneva-system amplitude ratios for the SPB class, as predicted by the modelling. The standard approach of obtaining these ratios (e.g. Heynderickx et al. 1994) is to normalize the light amplitude in each passband with that in the bluemost band, since the latter is generally the largest and best determined in observations. Thus, using

$$\mathcal{A}_{[x,U]} \equiv \mathcal{A}_x/\mathcal{A}_U, \tag{10}$$

as a shorthand for the ratio between the light amplitude in band *x* and that in the *U* band, $\mathcal{A}_{[x,U]}$ was calculated in the $x = \{U, B_1, B, B_2, V_1, V, G\}$ Geneva passbands, for each unstable mode found previously.

Given the multitude of unstable modes considered (~33 000), it would be unrealistic to present the ratio data of every single one. Therefore, for each harmonic degree and evolutionary sequence considered, three modes were selected as representative of the statistical properties of the data. The first of these 'characteristic modes', henceforth denoted C, was selected as that which

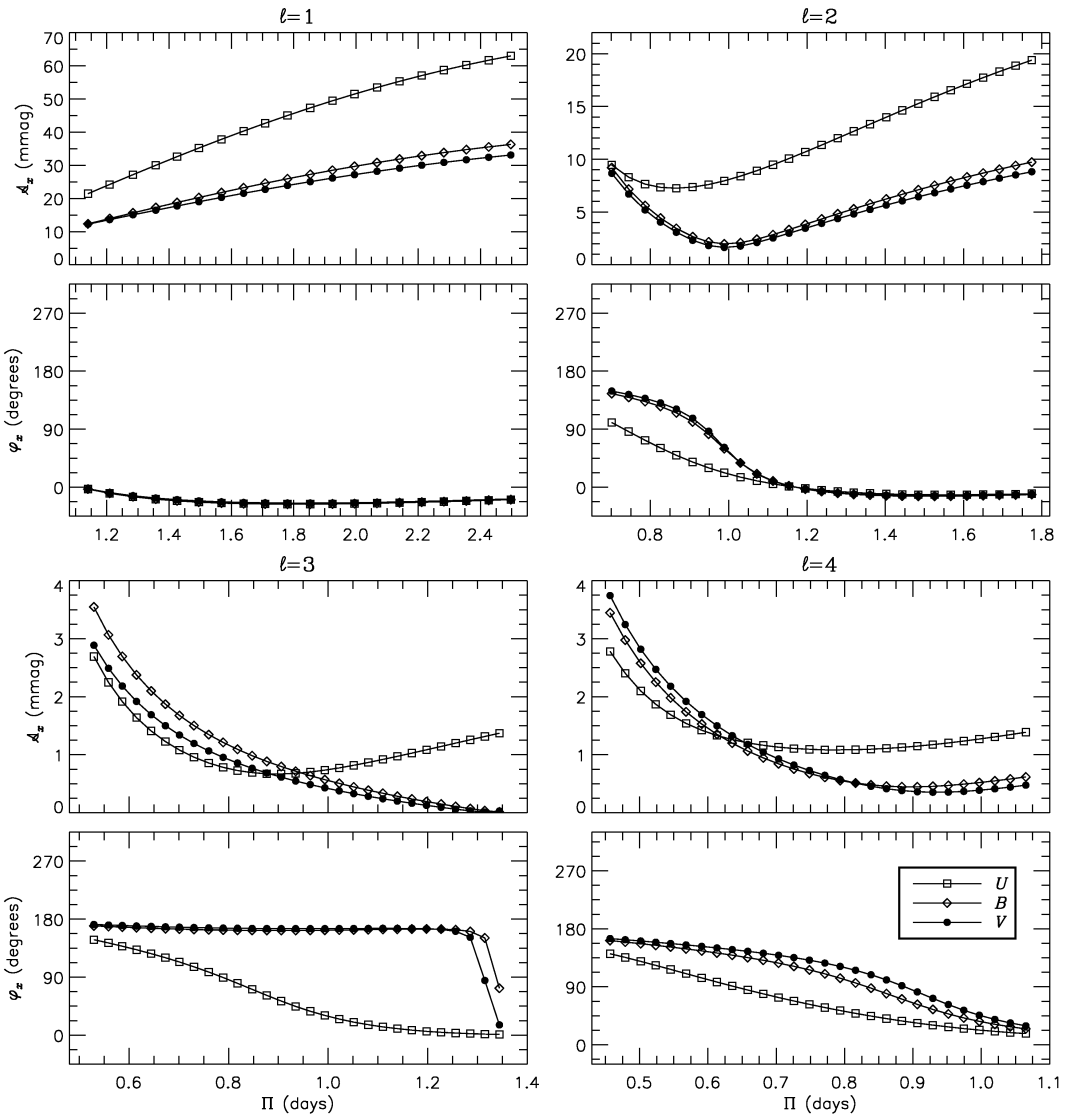

Figure 5. The cosinusoidal semi-amplitude $\mathcal{A}_x$ and phase φ_x, as a function of pulsation period Π, of light variations in the U (open squares), B (open diamonds) and V (filled circles) bands of the Geneva system, arising from unstable $\ell = 1\ldots4$ modes of the 4-$M_\odot$ stellar model.

minimized the discriminant

$$\mathcal{D} \equiv \sum_x [\mathcal{A}_{[x,U]} - \overline{\mathcal{A}_{[x,U]}}]^2; \tag{11}$$

here, the summation is taken over the seven Geneva passbands, and $\overline{\mathcal{A}_{[x,U]}}$ represents the mean value of $\mathcal{A}_{[x,U]}$ in passband x, averaged over all modes belonging to the same evolutionary sequence and harmonic degree. Evidently, C can be regarded as the mode with the amplitude ratio data 'closest' – in a least-squares sense – to the mean ratio in each passband.

The other two characteristic modes, denoted $C_{\sigma+}$ and $C_{\sigma-}$, were selected as the those which minimized the discriminants

$$\mathcal{D}_{\sigma+} \equiv \sum_x [\mathcal{A}_{[x,U]} - \overline{\mathcal{A}_{[x,U]}} - \sigma(\mathcal{A}_{[x,U]})]^2 \tag{12}$$

and

$$\mathcal{D}_{\sigma-} \equiv \sum_x [\mathcal{A}_{[x,U]} - \overline{\mathcal{A}_{[x,U]}} + \sigma(\mathcal{A}_{[x,U]})]^2, \tag{13}$$

respectively; here, $\sigma(\mathcal{A}_{[x,U]})$ (not to be confused with the pulsation frequency σ) represents the standard deviation of $\mathcal{A}_{[x,U]}$ in passband x, calculated once for all modes belonging to the same evolutionary sequence and harmonic degree. Hence, $C_{\sigma+}$ ($C_{\sigma-}$) may be regarded as the mode with ratio data 'closest' to the plus (minus) 1σ limit of the ratio in each passband.

Fig. 6 shows $\mathcal{A}_{[x,U]}$ for these triplets of characteristic modes, plotted against the mean wavelength of each passband x. As discussed in the preceding section, the amplitude ratios of $\ell = 1$ modes are primarily determined by the wavelength sensitivity of the temperature contributions, rather than by any particular properties of the pulsation. This explains why the characteristic modes in the $\ell = 1$ panels appear so similar, exhibiting a monotonic decline in $\mathcal{A}_{[x,U]}$ with increasing wavelength. Exceptions to such behaviour can be seen in the modes of the $M = 4.0$-$M_\odot$ and $M = 4.5$-$M_\odot$ panels, for which the decline in $\mathcal{A}_{[x,U]}$ is reversed (i.e. $\mathcal{A}_{[B_1,U]} < \mathcal{A}_{[B,U]} < \mathcal{A}_{[B_2,U]}$) around 4200 Å. It was found, in these particular cases, that the temperature perturbations were small enough for ITC to occur between the temperature and pressure contributions – a possibility suggested in Section 3.1. In a

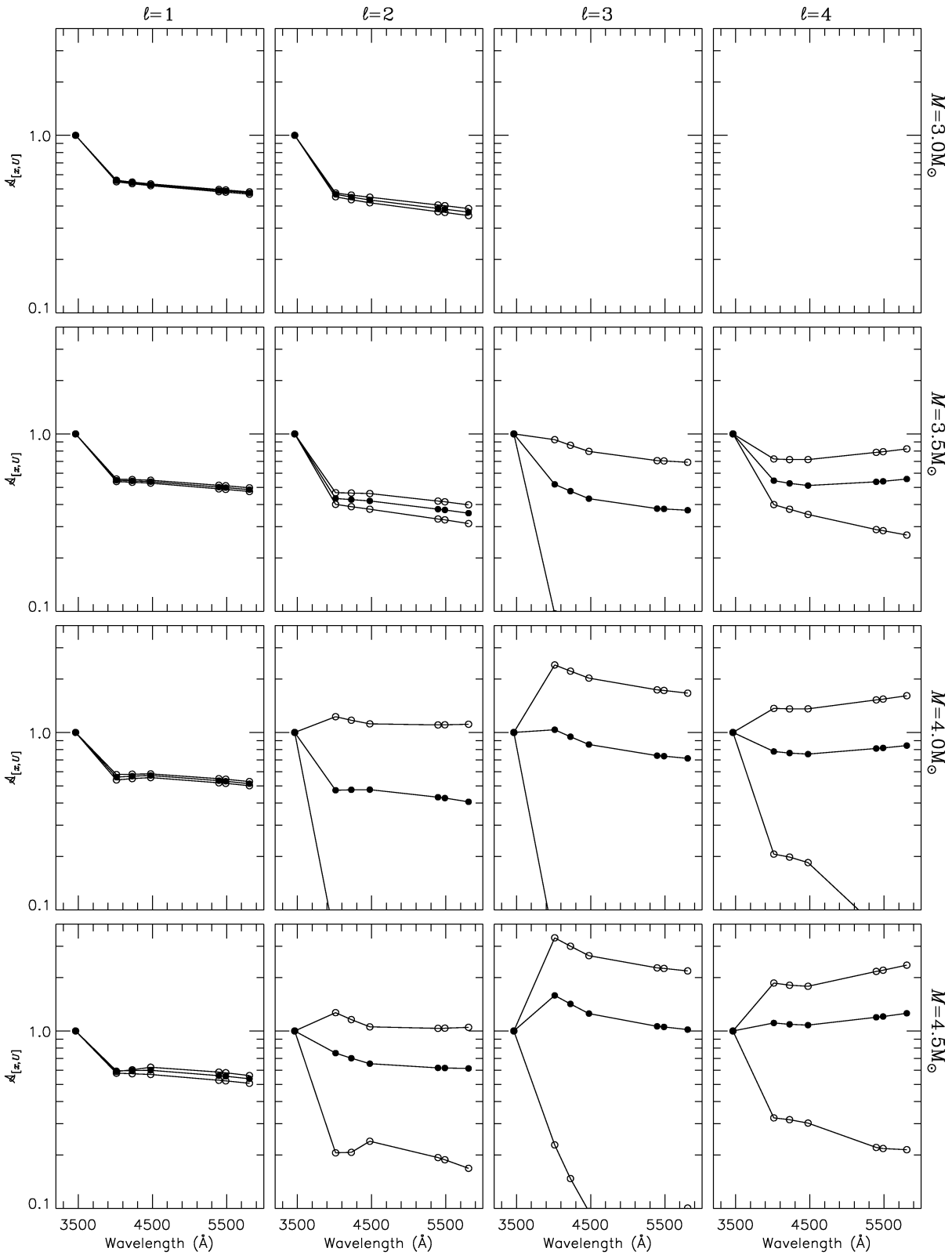

Figure 6. The amplitude ratios $\mathcal{A}_{[x,U]}$, plotted as a function of wavelength, for the $\ell = 1 \ldots 4$ triplets of characteristic modes belonging to the $M = 3.0 \ldots 4.5\text{-M}_\odot$ and $M = 5.0 \ldots 6.5\text{-M}_\odot$ evolutionary sequences; the data of the C modes are shown as filled circles, and those of the $C_{\sigma+}$ and $C_{\sigma-}$ as open circles. The two panels at the top right are blank because no $\ell = 3$ or $\ell = 4$ modes were unstable in the $M = 3.0\text{-M}_\odot$ sequence.

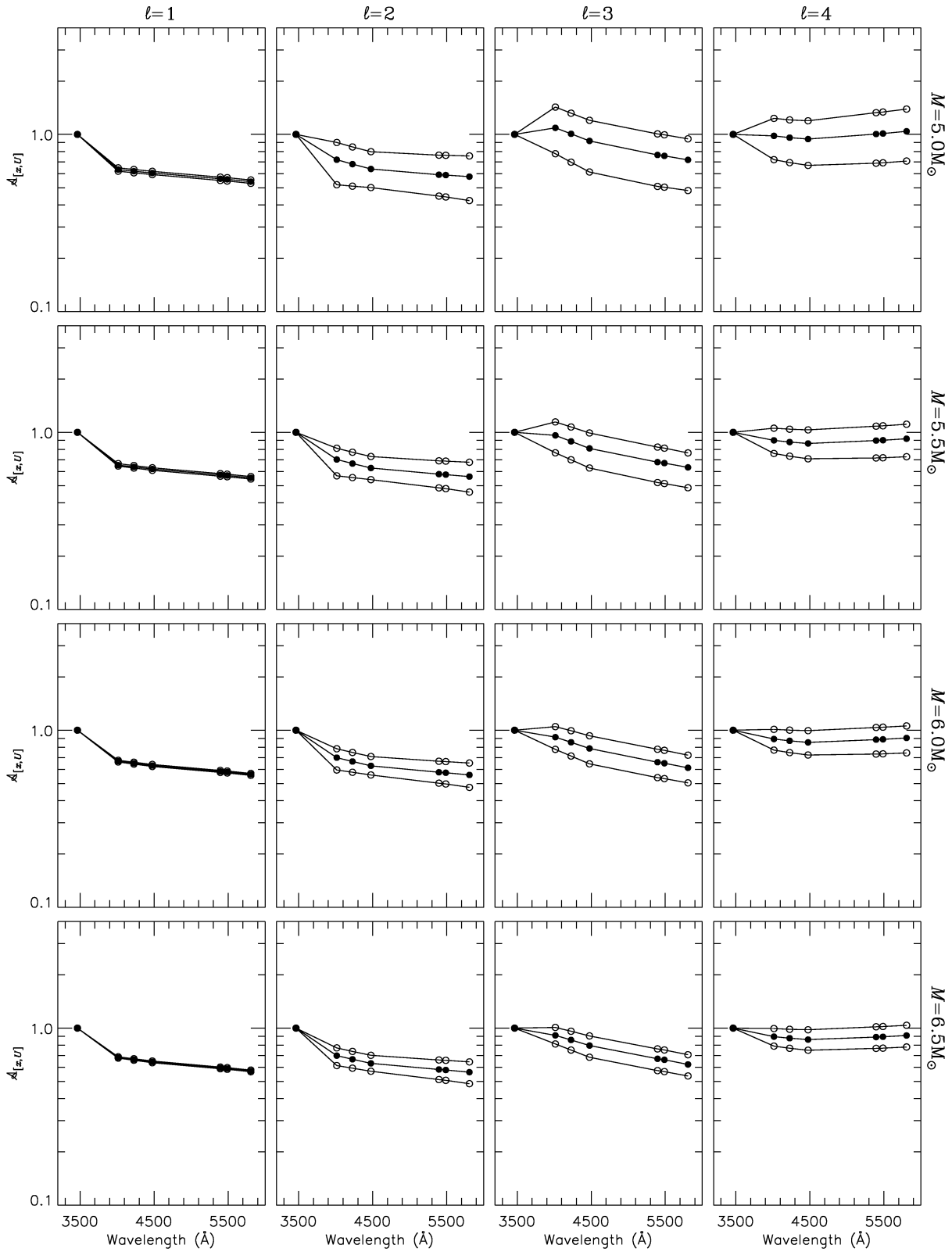

Figure 6 – *continued*

manner similar to that encountered for the shortest-period $\ell = 4$ modes of Fig. 5, this 'temperature-pressure' ITC leads to the reversal in the usual wavelength dependence of the $\ell = 1$ modes.

Inter-term cancellation, of the more familiar temperature–radius variety, explains the diverse behaviour seen in the $\ell = 2\ldots4$ panels of Fig. 6. From mode to mode, the degree of cancellation in each passband varies greatly, and significant differences can be seen between the behaviour of the C, $C_{\sigma+}$ and $C_{\sigma-}$ modes plotted in each panel. This is most evident in the intermediate-mass evolutionary sequences, for which the U-band ratio $\mathcal{A}_{[U,U]} \equiv 1$ is the largest – amongst the seven passbands – in the $C_{\sigma-}$ modes, but the smallest in the $C_{\sigma+}$ modes. In *all* sequences, the amplitude ratios in the redward (V_1, V, G) bands can be seen to grow with increasing harmonic degree; this is a consequence of the asymptotic period relationship $\Pi \propto [\ell(\ell+1)]^{-1/2}$ of g-modes (e.g. Unno et al. 1989, section 16), which means that higher degree modes pulsate at shorter periods. As demonstrated in the preceding section, cancellation in the U band is most pronounced at these shorter periods; therefore, the effect of incrementing ℓ is to reduce the light amplitude in the normalizing U band, and to raise by a corresponding amount the amplitude *ratios* of the redward bands.

Situations where the U-band amplitude was exceeded by that in one or more of the other bands were found to arise in over 50 per cent of the ~20 000 unstable $\ell = 3$ and $\ell = 4$ modes considered. This result should be contrasted with the fact that, amongst all recent observations of SPB stars, the same behaviour has only ever been recorded in a single star. It is uncertain whether this particular star, HD 55522, *is* actually undergoing non-radial pulsation; De Cat (2001) has suggested that its light variations may instead be a signature of the rotational modulation of a chemically inhomogeneous photosphere.

3.4 Amplitude–phase diagnostics

The principal strength of the multicolour-amplitudes technique developed by Heynderickx et al. (1994) lies in its ability to compare *simultaneously* the observed and theoretical light amplitudes in a multitude of passbands. However, the technique makes no use of the corresponding phase data: in their analysis of β Cephei stars, Heynderickx et al. (1994) made the ab initio assumption that the variations in each passband will always be in phase. This assumption, made on the basis of modelling by Saio & Cox (1980) which pre-dates the discovery of the metal-line instability, was demonstrated in Section 3.2 to be incorrect: calculations using up-to-date physics predict significant phase differences, for those modes strongly affected by ITC, between the variability in each band.

The nature of these phase differences is investigated further in this section, with the aid of an analysis technique developed by Stamford & Watson (1981). The technique centres around plotting the amplitude ratio against the phase difference, for the light variations in a given pair of passbands. As with the multicolour-amplitudes technique, a graphical comparison of observed and theoretically predicted plots may in principle be used as a discriminant for ℓ. Strictly speaking, Stamford & Watson (1981) considered colour-to-light amplitude ratios and phase differences; however, the approach described here is equally valid. Accordingly, let

$$\varphi_{[x,U]} \equiv \varphi_x - \varphi_U \tag{14}$$

denote the phase difference between the light variations in passband x and those in the U passband. Then, Figs 7 and 8 show the amplitude–phase diagrams – that is, $\mathcal{A}_{[x,U]}$ plotted against $\varphi_{[x,U]}$ – for the $U-B$ and $U-V$ pairs of passbands, respectively. Unlike Fig. 6, where only three characteristic modes were considered for each evolutionary sequence and harmonic degree, these figures include the data of *all* unstable modes.

The figures reveal that $\ell = 1$ modes tend to cluster around the $(\varphi_{[B,U]}, \mathcal{A}_{[B,U]}) \sim (0.0, 0.6)$ and $(\varphi_{[V,U]}, \mathcal{A}_{[V,U]}) \sim (0.0, 0.55)$ loci of the amplitude–phase planes. Although a small amount of scatter is seen in the 4.5-$M_\odot$ panel of the $U-V$ plane, owing to the temperature-pressure ITC discussed in Section 3.3, the clustering of the $\ell = 1$ modes remains reasonably tight across all eight evolutionary sequences. The same cannot be said of the $\ell = 2\ldots4$ modes, for which the incidence of ITC leads to significant scatter in the amplitude-ratio and phase-difference data. Notwithstanding the scatter, however, a number of trends can be recognized in these data. In particular, $\mathcal{A}_{[B,U]}$ tends to be systematically larger than $\mathcal{A}_{[V,U]}$, owing to the inverse wavelength dependence of the temperature contributions. Furthermore, in both pairs of passbands, there is an apparent correlation between stellar mass and phase difference. In the low-mass models, the modes tend to be confined to the $\varphi_{[B,U]}, \varphi_{[V,U]} > 0$ regions of the amplitude–phase plane, and the light variations in the U band lag those in the redward bands. The trend is reversed towards higher masses, with an increasing number of modes – ultimately, almost all – appearing in the $\varphi_{[B,U]}, \varphi_{[V,U]} < 0$ regions.

To understand this correlation, it should be noted that the phase of the temperature perturbations was found to lead that of the radius perturbations – that is, $\arg(\Delta_T) > \arg(\Delta_R)$ – for the majority of unstable $\ell = 2\ldots4$ modes in the low-mass models. However, the phase relationship is reversed in the more massive models, to such an extent that $\arg(\Delta_T) < \arg(\Delta_R)$ for *all* such modes of the 6.5-$M_\odot$ evolutionary sequence. When combined with the wavelength sensitivity of the temperature contributions (cf. Section 3.2), the aforementioned correspondence between M and phase difference emerges: $\varphi_{[B,U]}, \varphi_{[V,U]} < 0$ for the modes belonging to the $M \geqslant 5.0$-$M_\odot$ evolutionary sequences, and conversely for the $M \leqslant 4.0\,M_\odot$ sequences.

The intermediate-mass, $\ell = 2\ldots4$ panels of Figs 7 and 8 exhibit an interesting feature: the appearance of regions in the amplitude–phase plane where the concentration of modes is particularly high. Typically, these regions are situated around zero phase-difference, and take the form of cusps in the envelopes of the amplitude–phase data; a good example can be seen slightly below centre in the $M = 4.5$-$M_\odot$, $\ell = 2$ panels of both figures. The modes falling within these regions tend to be the ones excited at the short- or long-period boundaries of the κ-mechanism instability; because the light variations of such modes are largely unaffected by evolution of the underlying star (cf. Section 3.1), they accumulate around the same point within the amplitude–phase plane, leading to the behaviour noted.

Using results from their non-adiabatic stability calculations, Cugier et al. (1994) demonstrated that $\ell = 0\ldots2$ modes of β Cephei stars fall into disjoint regions of the amplitude–phase plane, facilitating the determination of the harmonic degrees responsible for observed variability. Evidently, the situation is somewhat more complicated for SPB stars. The incidence of ITC means that the regions of the amplitude–phase plane occupied by the $\ell = 2\ldots4$ modes, although reasonably distinct from those of the $\ell = 1$ modes, tend to overlap with one another, especially in the intermediate-mass models. Therefore, in many cases it will be difficult to discriminate between the former modes. The difficulty

can partly be ameliorated by exploiting the wavelength dependence of temperature contributions (cf. Section 3.2): comparison of Figs 7 and 8 reveals that, because of this dependence, the overlap is different in the $U-B$ and $U-V$ passbands. Accordingly, application of the amplitude–phase technique to the SPB class, while certainly tricky, can be more profitable if the amplitude–phase diagrams for more than one pair of passbands are considered. This approach is adopted in the following section, to establish limits on the harmonic degrees of modes observed in a number of SPB stars.

4 COMPARISON WITH OBSERVATIONS

Although this paper adopts a largely theoretical perspective, it is ultimately directed toward the observational community. Accordingly, a confrontation between the results of modelling and data obtained from observations of SPB variability is appropriate. Fig. 9 shows – for the four different values of ℓ considered – the complete set of synthetic amplitude–phase data, in both the $U-B$ and $U-V$ pairs of passbands. Overplotted are the corresponding data of the periodic variations detected by North & Paltani (1994) and De Cat & Aerts (in preparation) during Geneva-system observations of 14 different SPB stars. The observations of Waelkens (1991) have not been considered, owing to the lack of error estimates on his data.

As mentioned in Section 3.2, North & Paltani (1994) cited the absence of significant phase differences between the light variations in each band as a defining characteristic of SPB stars. Clearly, the observational data plotted in Fig. 9 conform to this characterization: all modes fall within the limits $|\varphi_{[B,U]}| < 15°$ and $|\varphi_{[V,U]}| < 18°$. However, the same cannot be said for the synthetic $\ell = 3$ and $\ell = 4$ modes: the majority exhibit much larger phase differences, and on these grounds may be ruled out as responsible for the variability. Of the remainder in which both $\varphi_{[B,U]}$ and $\varphi_{[V,U]}$ are small, the amplitude ratios are generally inconsistent, in one or both of the passband pairs, with those observed. Accordingly – with the exception of a couple of marginal $\ell = 4$ cases – it would appear that the observations cannot be reconciled with an $\ell = 3$ or $\ell = 4$ identification.

It would be tempting to conclude from Fig. 9 that the observed variability is therefore caused primarily by a combination of $\ell = 1$ and $\ell = 2$ modes. Certainly, the observations plotted in the figure appear to be consistent with the synthetic data of these modes, with the only exception – seen as an outlier towards the upper-right of the $U-B$ panels – being HD 53921 [the variations of this star are already known (De Cat 2001) to be difficult to reconcile with models of non-radial pulsation]. However, it must be stressed that the figure provides necessary rather than sufficient evidence to support such a mode identification. Specifically, there is no way to tell which datum in the $U-V$ amplitude–phase plane represents the same mode as a given datum in the $U-B$ plane. This highlights one of the notable limitations of the amplitude–phase technique: it is not easy to consider, simultaneously, the data from more than one pair of passbands. Contrast this shortcoming with that of the multicolour-amplitudes technique, which permits the simultaneous comparison of amplitude data across a multitude of passbands, but makes no use whatsoever of the corresponding phase data.

While it certainly appears *likely* that the fourteen SPB stars considered are pulsating in $\ell = 1$ or $\ell = 2$ modes, with the marginal possibility of $\ell = 4$ modes in a few cases, more intensive modelling is required to support such a conclusion. In particular, the simultaneous reproduction of amplitude *and* phase data, across *all* passbands, will have to be secured before any reliable mode identifications can be advanced. Furthermore, it will be necessary to restrict the analysis to stellar models with physical parameters that match those of the stars observed, rather than – as in Fig. 9 – considering all models that fall within the SPB instability strip. Accordingly, a follow-up paper is planned, in which mode identifications in the manner described will be undertaken for the SPB observations considered in this section.

5 CONCLUSIONS

In this paper, photometric data have been synthesized for a range of mid-B type stellar models, using input parameters derived from non-adiabatic stability calculations. These data, visualized and discussed using a variety of approaches, have revealed two important properties of the SPB class of non-radial pulsators. First, based on the approximate limits established in Section 3.1 for the maximum amplitude of light variations, it has been found that the photometric detection of $\ell \geqslant 5$ modes in these systems probably lies beyond the capabilities of present-day instrumentation. Such modes suffer greatly from disc-averaging cancellation, and – even when pulsating at large amplitudes – exhibit little photometric variability. The situation can be expected to change with the commissioning of upcoming space-based observatories (see, e.g. Eyer 2000), which will be able to measure flux variations at micromagnitude levels; however, observations using current facilities are probably limited to the detection of $\ell \leqslant 4$ modes.

Secondly, it has been discovered that inter-term cancellation – the process of destructive interference between the light variations generated by a pair of perturbative mechanisms – plays a key role in determining the photometric characteristics of SPB stars. The concept of ITC was originally suggested by Watson (1987); however, the present analysis demonstrates the importance of using quantitative non-adiabatic parameters if the phenomenon is to be modelled correctly. Two variants of ITC have been encountered: between the temperature and radius contributions for $\ell \geqslant 2$ modes, and – to a much lesser extent – between the temperature and pressure contributions for $\ell = 1$ modes. Much like the aforementioned disc-averaging cancellation, the effect of ITC is to reduce the light variations exhibited by a star; however, because of the wavelength dependence of the temperature contributions, the degree of the reduction varies between differing passbands.

Accordingly, the chances of overlooking a mode as a consequence of ITC can greatly be reduced by examining light variations in two or (preferably) more passbands. Regrettably, of the sample of ~100 SPB stars known to date, the majority were discovered (Waelkens et al. 1998) from observations in a single passband – the broad-band H_p filter of the *Hipparcos* satellite. Although accompanying measurements were obtained in the two narrower filters of the *Tycho* star mapper (see Perryman 1997), independent searches for variability in these latter data have proven difficult (Friedrich, Koenig & Wicenec 1997). Therefore, it is possible that the current sample of known SPB stars may be biased against those modes most strongly affected by cancellation in the H_p passband. Such a bias would certainly have to be taken into account in any statistical analyses of the SPB class.

In addition to reducing the amplitude of light variations, ITC greatly leverages their sensitivity towards mode-to-mode changes in the underlying pulsation. Because the degree of this leverage is unique to each passband, the modes most affected by ITC – primarily, those in intermediate-mass SPB stars – exhibit

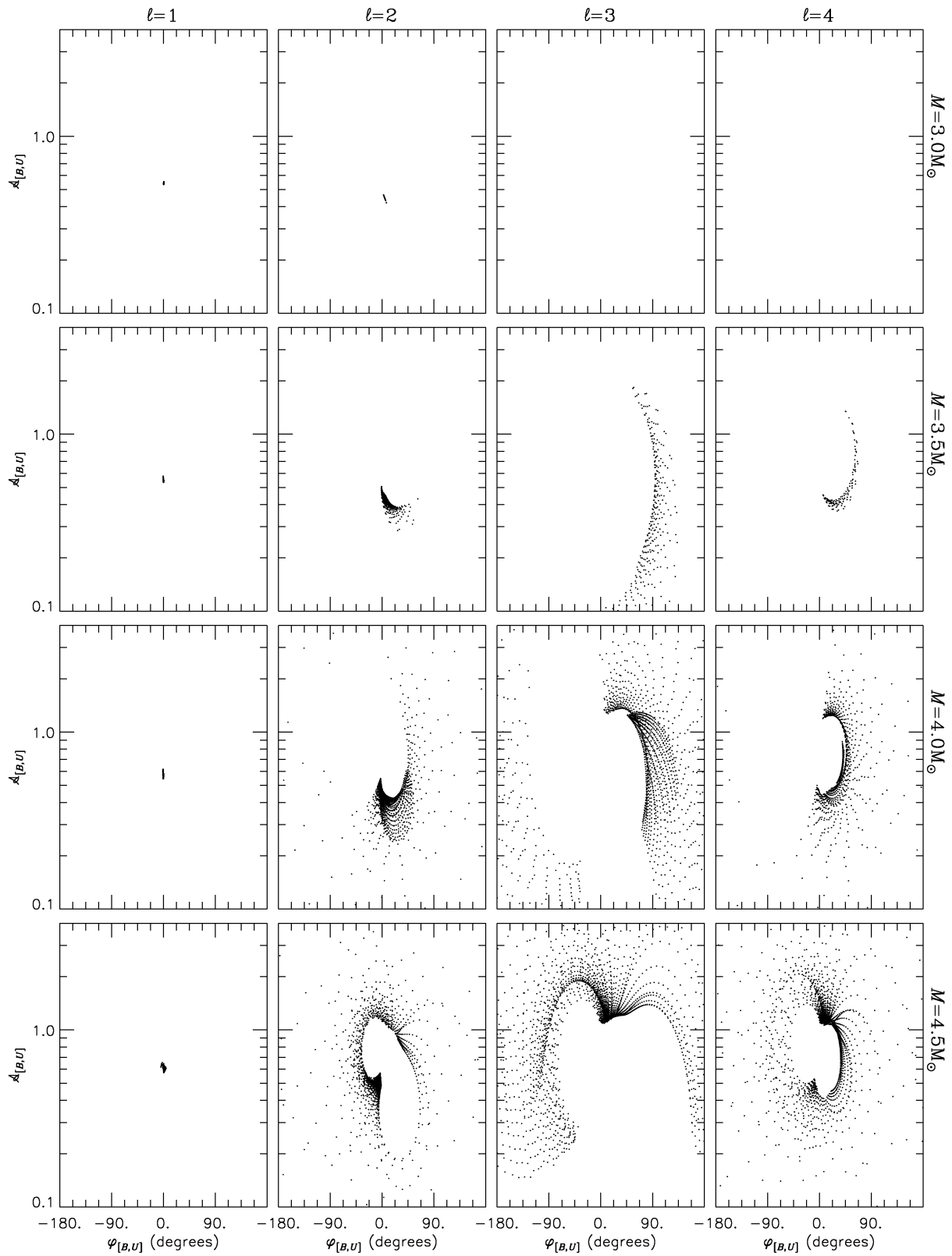

Figure 7. The $U - B$ amplitude ratio $\mathcal{A}_{[B,U]}$ plotted against the corresponding $U - B$ phase difference $\varphi_{[B,U]}$, for the unstable $\ell = 1 \ldots 4$ modes belonging to the $M = 3.0 \ldots 4.5\text{-M}_\odot$ and $M = 5.0 \ldots 6.5\text{-M}_\odot$ evolutionary sequences; each mode is shown as a point in the amplitude–phase plane. The two panels at the top right are blank because no $\ell = 3$ or $\ell = 4$ modes were unstable in the $M = 3.0\text{-M}_\odot$ sequence.

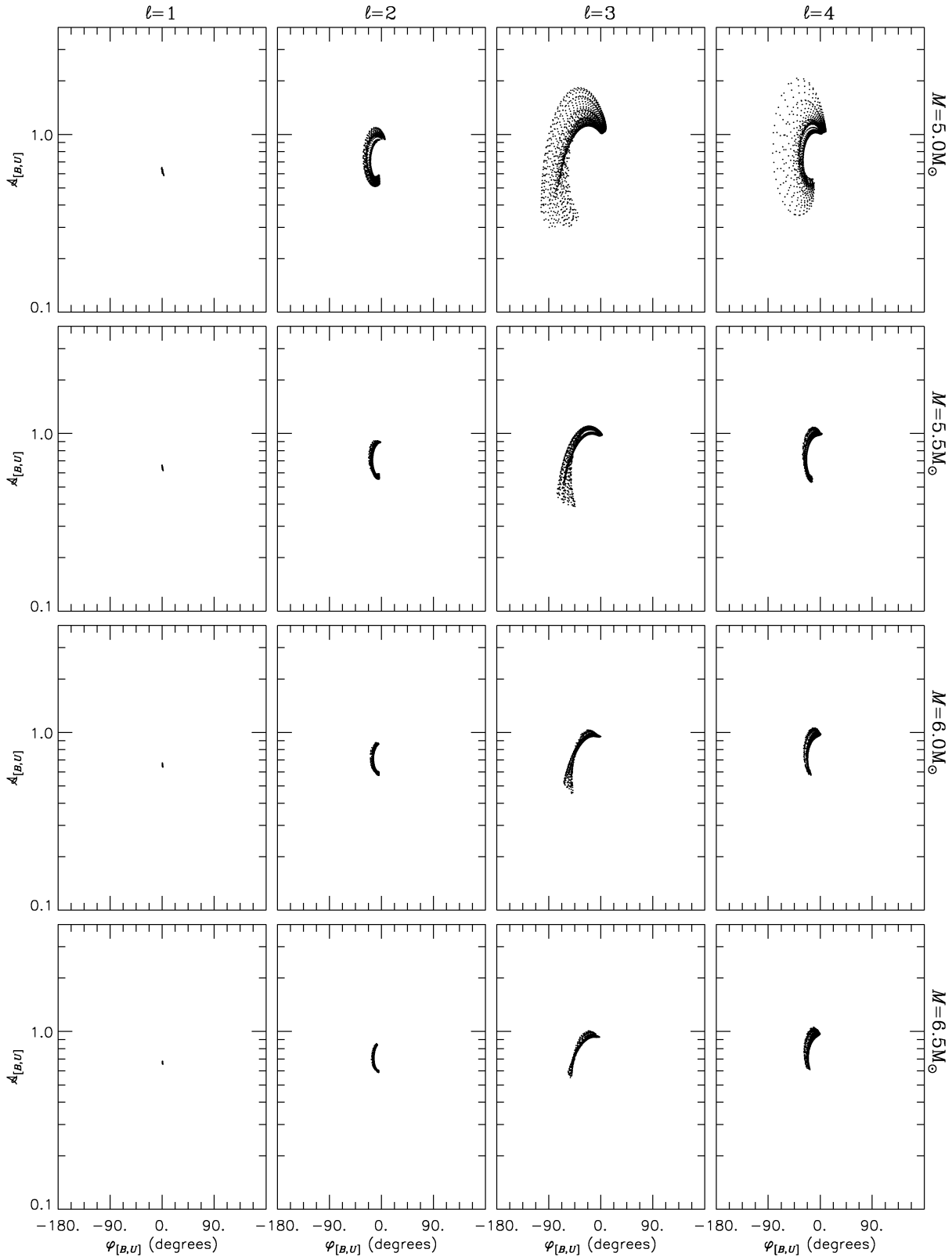

Figure 7 – *continued*

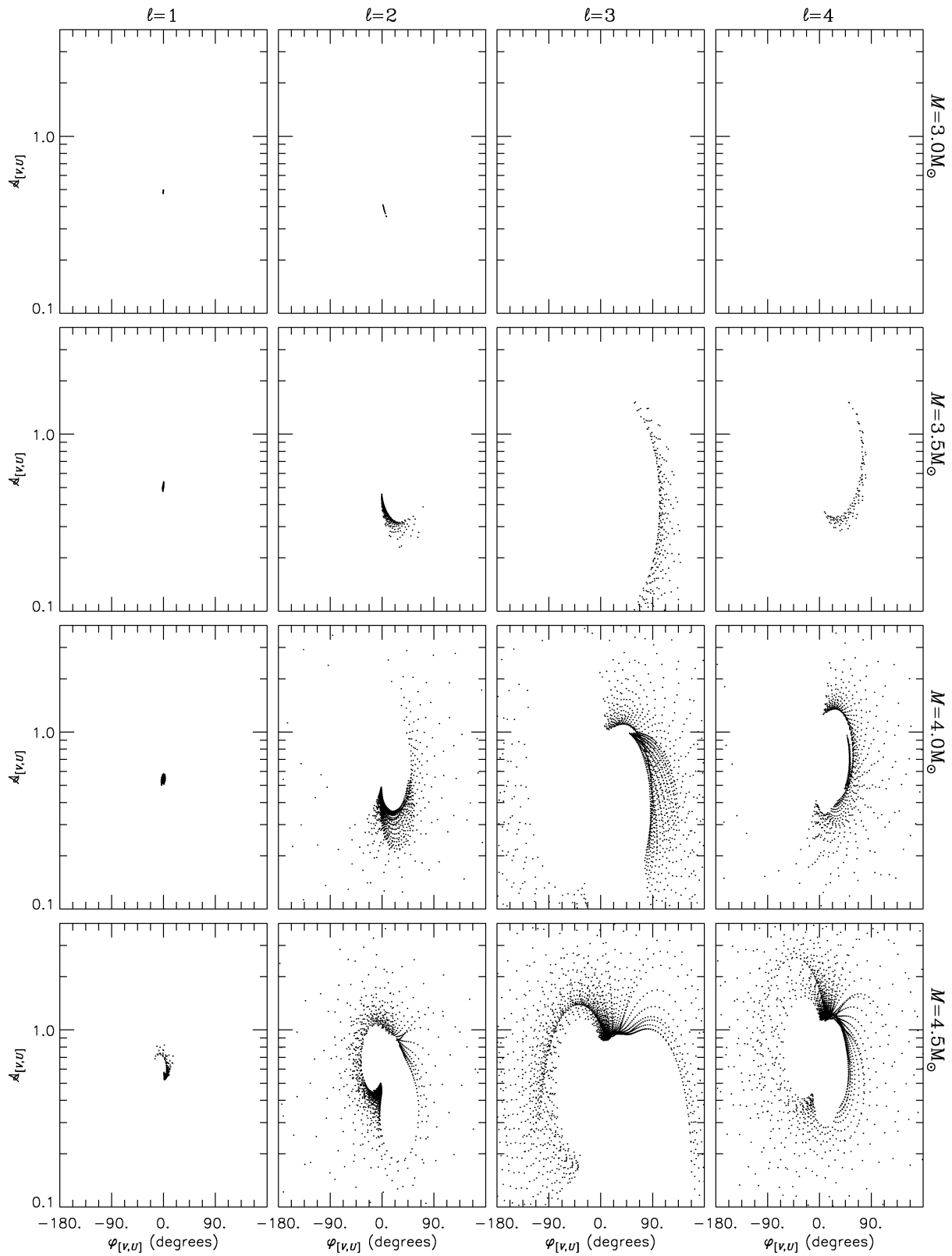

Figure 8. The $U - V$ amplitude ratio $\mathcal{A}_{[V,U]}$ plotted against the corresponding $U - V$ phase difference $\varphi_{[V,U]}$, for the unstable $\ell = 1 \ldots 4$ modes belonging to the $M = 3.0 \ldots 4.5\text{-M}_\odot$ and $M = 5.0 \ldots 6.5\text{-M}_\odot$ evolutionary sequences; each mode is shown as a point in the amplitude–phase plane. The two panels at the top right are blank because no $\ell = 3$ or $\ell = 4$ modes were unstable in the $M = 3.0\text{-M}_\odot$ sequence.

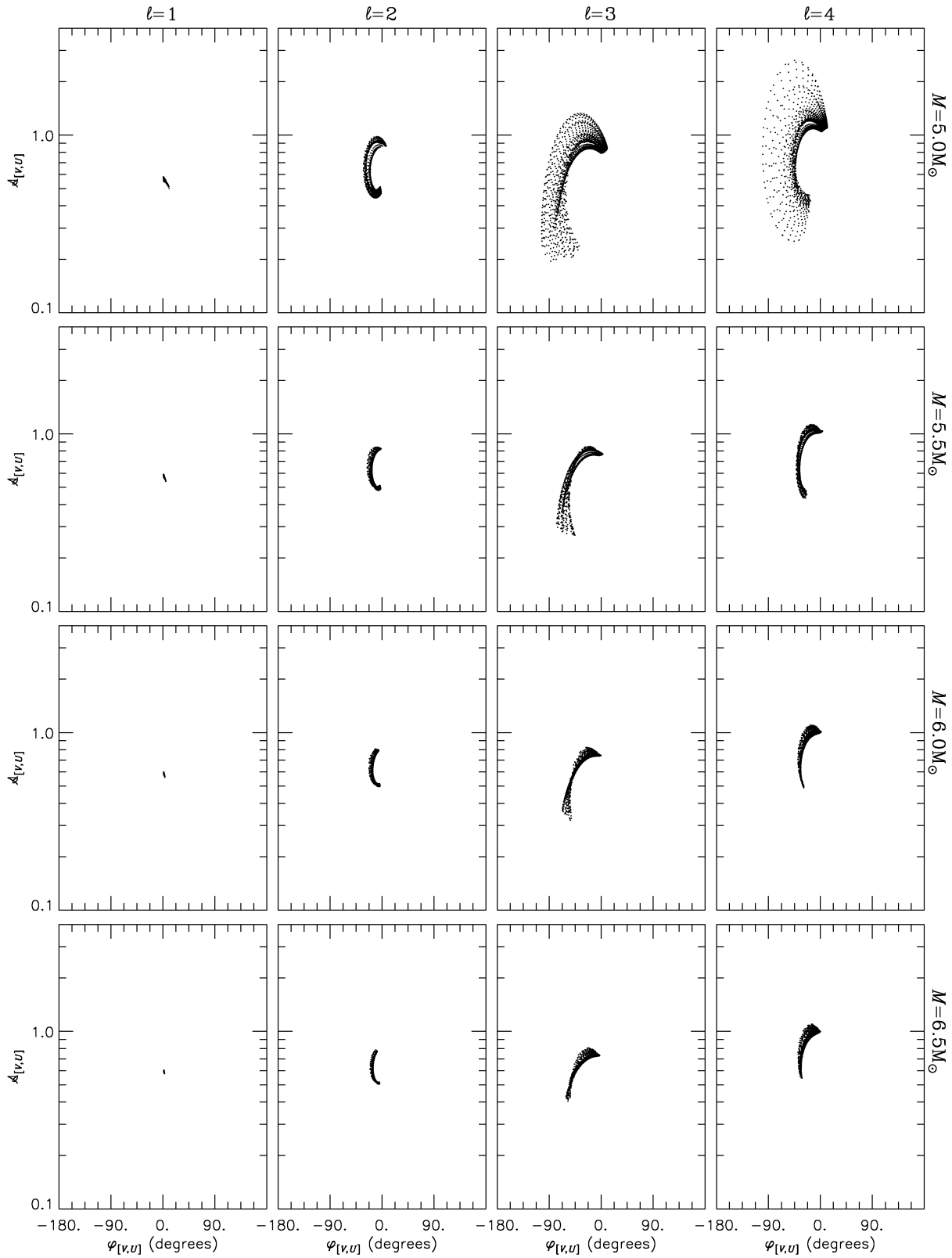

Figure 8 – *continued*

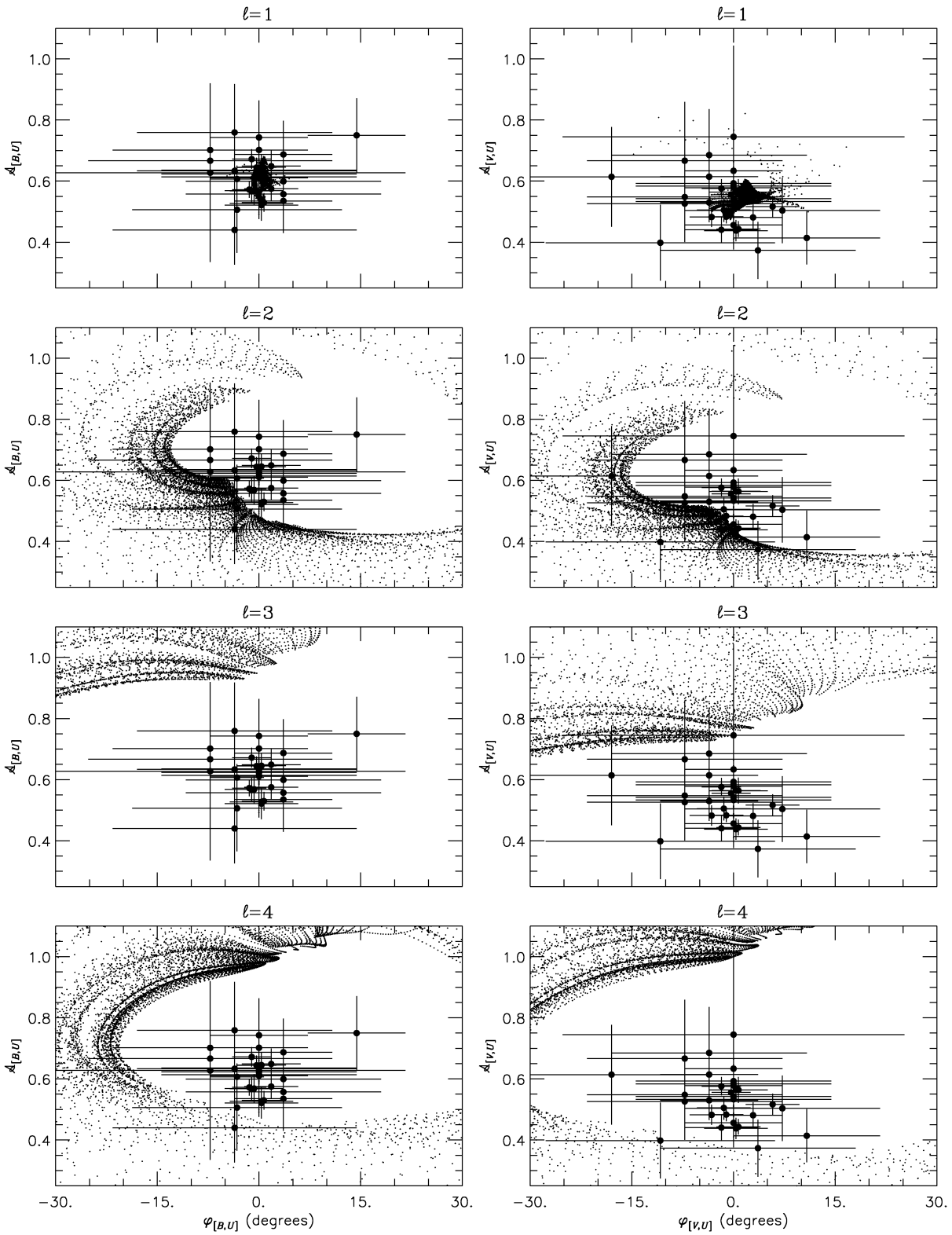

Figure 9. The amplitude ratio $\mathcal{A}_{[x,U]}$ (small points), plotted against the phase difference φ_x for the unstable $\ell = 1 \ldots 4$ modes considered throughout, of light variations in the $U - B$ (left) and $U - V$ (right) pairs of passbands. Overplotted (filled circles) are the data for the modes observed in HD 123515, 140873, 24587, 53921, 74560, 177863, 92287, 74195, 181558, 26326, 85953, 138764, 215573 (De Cat & Aerts, in preparation) and 37151 (North & Paltani 1994). Measurement errors for the latter are indicated by the vertical and horizontal bars.

significant scatter in their amplitude-ratio and phase-difference data. The scatter complicates any attempts at discrimination between modes of harmonic degrees $\ell = 2..4$ using the well-established Stamford & Watson (1981) and Heynderickx et al. (1994) techniques. Nevertheless, the observational characteristics of these modes remain quite distinct from those of the $\ell = 1$ modes, and it should remain straightforward to distinguish between the former and the latter.

The last point explains the partial success achieved in the preceding section at constraining the harmonic degrees of the various SPB modes detected by North & Paltani (1994) and De Cat & Aerts (in preparation). In all but a few marginal cases, an $\ell = 3$ or $\ell = 4$ identification could be ruled out; for these values of the harmonic degree, the synthetic data exhibit large phase differences between the variability in each band, in contradiction to the small or non-existent phase differences seen in the observational data. Underpinning this result is perhaps the most important conclusion to be drawn from the paper: photometric modelling of SPB stars *must* focus around the reproduction of observed amplitude *and* phase data. The consideration of amplitude data alone is insufficient.

ACKNOWLEDGMENTS

I thank Ryszard Sienkiewicz for the generous provision of the Warsaw–New Jersey code, and the anonymous referee for many useful remarks. Thanks must also go to Ian Howarth and the A25 society for their valuable input. This research has been supported by the Particle Physics and Astronomy Research Council of the UK, and has made use of Starlink computer facilities and the on-line ADS Abstract Service.

NOTE ADDED IN PROOF

It has come to the attention of the author that the normalization condition (1) was implemented incorrectly in the NARK code. As a result, the photometric amplitudes calculated throughout the paper are too small, by a factor of $\sqrt{(4\pi)}$. This error will influence the upper limits on the photometric amplitudes, as discussed in Section 3.1. However, the subsequent sections, and the conclusions of the paper as a whole, will remain unaffected.

REFERENCES

Allen C. W., 1976, Astrophysical Quantities. 3rd edn. Athlone, London
Ando H., Osaki Y., 1975, PASJ, 27, 581
Balona L. A., Dziembowski W. A., 1999, MNRAS, 309, 221
Balona L. A., Evers E. A., 1999, MNRAS, 302, 349
Balona L. A., Stobie R. S., 1979, MNRAS, 189, 649
Bessell M. S., 1990, PASP, 102, 1181
Buta R. J., Smith M. A., 1979, ApJ, 232, 213
Cox A. N., Morgan S. M., Rogers F. J., Iglesias C. A., 1992, ApJ, 393, 272
Cugier H., Dziembowski W. A., Pamyatnykh A. A., 1994, A&A, 291, 143
De Cat P., 2001, PhD thesis, Katholieke Universiteit Leuven
Dupret M. A., 2001, A&A, 366, 166
Dziembowski W. A., 1971, Acta Astron., 21, 290
Dziembowski W. A., 1977, Acta Astron., 27, 203
Dziembowski W. A., Pamyatnykh A. A., 1993, MNRAS, 262, 204
Dziembowski W. A., Moskalik P., Pamyatnykh A. A., 1993, MNRAS, 265, 588
Eyer L., 2000, in Szabados L., Kurtz D. W., eds, Proc IAU Colloq. 176, The Impact of Large-Scale Surveys on Pulsating Star Research. Astron. Soc. Pac., San Francisco, p. 41
Friedrich S., Koenig M., Wicenec A., 1997, in Perryman M. A. C., Bernacca P. L., eds, ESA SP-402, Hipparcos – Venice '97. ESA, Noordwijk, p. 441
Gautschy A., 2000, in Szabados L., Kurtz D. W., eds, Proc IAU Colloq. 176, The Impact of Large-Scale Surveys on Pulsating Star Research. Astron. Soc. Pac., San Francisco, p. 325
Grevesse N., Noels A., 1993, in Pratzo N., Vangioni-Flam E., Casse M., eds, Origin and Evolution of the Elements. Cambridge University Press, Cambridge, p. 15
Heynderickx D., Waelkens C., Smeyers P., 1994, A&AS, 105, 447
Iglesias C. A., Rogers F. J., 1996, ApJ, 464, 943
Kurucz R., 1993, CD-ROM No. 16: Limb darkening for 2 km/s grid. Smithsonian Astrophys. Obs., Cambridge MA
Matsushima S., 1969, ApJ, 158, 1137
North P., Paltani S., 1994, A&A, 288, 155
Pamyatnykh A. A., 1999, Acta Astron., 49, 119
Perryman M. A. C., 1997, ESA SP-1200: The Hipparcos and Tycho catalogues. ESA, Netherlands
Rogers F. J., Swenson F. J., Iglesias C. A., 1996, ApJ, 456, 902
Rufener F., Nicolet B., 1988, A&A, 206, 357
Saio H., Cox J. P., 1980, ApJ, 236, 549
Smith M. A., 1977, ApJ, 215, 574
Stamford P. A., Watson R. D., 1981, Ap&SS, 77, 131
Townsend R. H. D., 1997, PhD thesis, Univ. London
Unno W., Osaki Y., Ando H., Saio H., Shibahashi H., 1989, Nonradial oscillations of stars. 2nd edn. University of Tokyo Press, Tokyo
Unno W., Spiegel E. A., 1966, PASJ, 18, 85
Waelkens C., 1991, A&A, 246, 453
Waelkens C., Rufener F., 1985, A&A, 152, 6
Waelkens C., Aerts C., Kestens E., Grenon M., Eyer L., 1998, A&A, 330, 215
Watson R. D., 1987, Publ. Astron. Soc. Austr., 7, 38
Watson R. D., 1988, Ap&SS, 140, 255

This paper has been typeset from a TEX/LATEX file prepared by the author.